

Helsinki University of Technology  
Inorganic Chemistry Publication Series  
Espoo 2001 No. 1

## **DEPOSITION OF BINARY AND TERNARY OXIDE THIN FILMS OF TRIVALENT METALS BY ATOMIC LAYER EPITAXY**

**Minna Nieminen**

Dissertation for the degree of Doctor of Science in Technology to be presented with due permission of the Department of Chemical Technology for public examination and debate in Auditorium KE 2 (Komppa Auditorium) at Helsinki University of Technology (Espoo, Finland) on the 7th of December, 2001, at 12 noon.

Helsinki University of Technology  
Department of Chemical Technology  
Laboratory of Inorganic and Analytical Chemistry

Teknillinen korkeakoulu  
Kemian tekniikan osasto  
Epäorgaanisen ja analyttisen kemian laboratorio

Distribution:  
Helsinki University of Technology  
Laboratory of Inorganic and Analytical Chemistry  
P.O.Box 6100  
FIN-02015 HUT

© Minna Nieminen

ISBN 951-22-5747-5  
ISSN 1458-5154

Picaset Oy  
Helsinki 2001

## ABSTRACT

The atomic layer epitaxy (ALE) technique was used to grow thin films of binary metal oxides  $\text{Al}_2\text{O}_3$ ,  $\text{Ga}_2\text{O}_3$  and  $\text{La}_2\text{O}_3$ , and ternary metal oxides  $\text{LaNiO}_3$ ,  $\text{LaCoO}_3$ ,  $\text{LaAlO}_3$ , and  $\text{LaGaO}_3$ . In addition, another type of mixed-oxide, *viz.* phosphorus-doped  $\text{Al}_2\text{O}_3$  was studied. The binary oxides  $\text{Ga}_2\text{O}_3$  and  $\text{La}_2\text{O}_3$  and all the ternary oxides were deposited by the ALE method for the first time. New ALE processes were developed for the undoped and doped  $\text{Al}_2\text{O}_3$  films. The thin films were characterized by a wide range of methods for structural and surface analysis, including XRD, FTIR, XPS, AFM, XRF, RBS, TOF-ERDA, and SIMS. A review of previous work on these trivalent metal oxide thin films is presented by way of background.

The  $\text{Al}_2\text{O}_3$  and  $\text{Ga}_2\text{O}_3$  films deposited from metal beta-diketonates and ozone were of high quality: stoichiometric, uniform, dense, and free of any significant contamination. However, the  $\text{La}_2\text{O}_3$  films contained an excess of oxygen, due to the carbonate-type impurity that was detected. All  $\text{Al}_2\text{O}_3$  and  $\text{Ga}_2\text{O}_3$  films were amorphous, but polycrystalline, cubic  $\text{La}_2\text{O}_3$  was formed at temperatures above 300 °C. Hexagonal  $\text{La}_2\text{O}_3$  film was obtained by annealing the as-deposited amorphous and cubic  $\text{La}_2\text{O}_3$  films. Simultaneously, the carbon content in the films was reduced. In contrast to the stable  $\text{Al}_2\text{O}_3$  and  $\text{Ga}_2\text{O}_3$  films, the cubic and hexagonal  $\text{La}_2\text{O}_3$  films were chemically unstable and reacted with ambient air, transforming to  $\text{LaO}(\text{OH})$  and  $\text{La}(\text{OH})_3$ , respectively.

The perovskite-type oxides  $\text{LaNiO}_3$ ,  $\text{LaCoO}_3$ ,  $\text{LaAlO}_3$ , and  $\text{LaGaO}_3$  were deposited using metal beta-diketonates and ozone as precursors. No optimal ALE process could be demonstrated for the  $\text{LaNiO}_3$  and  $\text{LaCoO}_3$  films, which were non-uniform in thickness and either consisted of separate oxide layers or contained an excess of the transition metal. The  $\text{LaAlO}_3$  and  $\text{LaGaO}_3$  film growth, in contrast, was well-controlled yielding stoichiometric, uniform, and smooth films, demonstrating the potential of the ALE technique for producing the more complex ternary oxide films.

All the as-deposited ternary oxide films were amorphous but crystallized with cubic structure when post-annealed *ex situ*. After annealing high-quality, epitaxial  $\text{LaAlO}_3$  and  $\text{LaGaO}_3$  films were obtained on lattice-matched perovskite-type substrates while randomly or slightly oriented films were obtained on non-lattice matched substrates. The films were relatively pure and only small amounts of common impurities, carbon and hydrogen, were detected.

Phosphorus-doped  $\text{Al}_2\text{O}_3$  films were deposited from  $\text{AlCl}_3$ ,  $\text{P}_2\text{O}_5$  or trimethylphosphate, and water. The phosphorus content could be controlled by the phosphorus doping ratio: when the P/Al atomic ratio was below 1.0, the films consisted of both  $\text{Al}_2\text{O}_3$  and  $\text{AlPO}_4$ , whereas above that they contained predominantly  $\text{AlPO}_4$ . Phosphorus was uniformly distributed when the phosphorus content exceeded 5 at.%, and it was enriched on the film/substrate interface when the content was lower.

## **PREFACE**

This thesis is based on the experimental work carried out in the Laboratory of Inorganic and Analytical Chemistry, Helsinki University of Technology, during the years 1994-1996 and 1999-2001.

I wish to express my deep gratitude to my supervisor Professor Lauri Niinistö for his support, encouragement and advice during this work.

I would like to thank my coauthors Dr. Helene Seim and Dr. Hjelmer Fjellvåg for introducing me to the perovskite-type oxide materials and fruitful co-operation. I am also very grateful for the help of, present and past, members of the ALE thin film group at the Laboratory of Inorganic and Analytical Chemistry. Particularly I would like to express my thanks to my research colleagues and coauthors Ms. Heini Mölsä and Mr. Matti Putkonen for their contributions in thin film preparations and analyses as well as useful comments. For technical help and assistance, I wish to acknowledge Mrs. Anita Pirhonen, Mr. Pekka Hassinen and Mr. Lassi Hiltunen. The whole personnel in the Laboratory of Inorganic and Analytical Chemistry are thanked for all their help.

During this work, I had the pleasure of working with many skillful scientists, without whom the comprehensive characterization of the thin films would not have been possible. I am greatly indebted to my coauthors Doc. Eero Rauhala, Dr. Reijo Lappalainen and Mr Timo Sajavaara for the RBS and TOF-ERDA analyses and Dr. Leena-Sisko Johansson for the XPS analyses. Very special thanks I owe to Dr. Sari Lehto for the SIMS analyses and also for her support and valuable comments during the preparation of the manuscript of this thesis. I am further grateful to Mr Jaakko Niinistö for AFM measurements and to Mr Antti Niskanen for rocking curve measurements. Dr. Kathleen Ahonen is thanked for revising the language of this thesis.

The Academy of Finland, the Foundation of Technology and Jenny and Antti Wihuri Foundation are acknowledged for the financial support.

My warmest thanks belong to my family, especially my mother Laila Nieminen, and my friends for their support.

Espoo, October 2001

Minna Nieminen

## LIST OF PUBLICATIONS

In addition to the present review, the dissertation includes the following publications, which are referred to in the text by the corresponding Roman numerals:

- I Nieminen, M., Niinistö, L., and Lappalainen, R.,  
Determination of P/Al ratio in phosphorus-doped aluminium oxide thin films by XRF, RBS and FTIR,  
*Mikrochim.Acta* **119** (1995) 13-22.
- II Nieminen, M., Niinistö, L., and Rauhala, E.,  
Growth of gallium oxide thin films from gallium acetylacetonate by atomic layer epitaxy,  
*J.Mater.Chem.* **6** (1996) 27-31.
- III Nieminen, M., Putkonen, M., and Niinistö, L.,  
Formation and stability of La<sub>2</sub>O<sub>3</sub> thin films deposited from β-diketonate precursor,  
*Appl.Surf.Sci.* **174** (2001) 155-165.
- IV Seim, H., Mölsä, H., Nieminen, M., Fjellvåg, H., and Niinistö, L.,  
Deposition of LaNiO<sub>3</sub> thin films in an atomic layer epitaxy reactor,  
*J.Mater.Chem.* **7** (1997) 449-455.
- V Seim, H., Nieminen, M., Niinistö, L., Fjellvåg, H., and Johansson, L.-S.,  
Growth of LaCoO<sub>3</sub> thin films from β-diketonate precursors,  
*Appl.Surf.Sci.* **112** (1997) 243-250.
- VI Nieminen, M., Sajavaara, T., Rauhala, E., Putkonen, M., and Niinistö, L.,  
Surface-controlled growth of LaAlO<sub>3</sub> thin films by atomic layer epitaxy,  
*J.Mater.Chem.* **11** (2001) 2340-2345.
- VII Nieminen, M., Lehto, S., and Niinistö, L.,  
Atomic layer epitaxy growth of LaGaO<sub>3</sub> thin films,  
*J.Mater.Chem.* (2001), in press.

## THE AUTHOR'S CONTRIBUTION

- Publications I and II      The research plan for the experimental work, all of the experiments and interpretation of the results, except the RBS analyses, and writing of the articles were done by the author.
- Publication III            The research plan for the experimental work and the interpretation of the results were made together with Mr. Matti Putkonen. The author did most of the experiments (ALE depositions and XRD and FTIR measurements as well as thickness determinations) and wrote the article.
- Publication IV            The author did part of the ALE depositions, thickness determinations and XRD measurements as well as participated in the interpretation of the results. The author had a minor role in writing the manuscript.
- Publication V            The author participated in the preparation of the research plan, experimental work, interpretation of the results and had a minor role in writing the manuscript.
- Publications VI and VII    The author made the research plans and most of the experiments as well as interpretation of the results, except the depositions of MgO buffer layers and TOF-ERDA, RBS, AFM, XPS, SIMS and rocking curve analyses. The author wrote the articles.

## LIST OF ABBREVIATIONS

acac	acetylacetonato = pentane-2,4-dionate
acim	acetylacetoniminate
AFM	Atomic force microscopy
ALCVD	Atomic layer chemical vapor deposition
ALD	Atomic layer deposition
ALG	Atomic layer growth
ALE	Atomic layer epitaxy
CMR	Colossal magnetoresistance
CSD	Chemical solution deposition
CVD	Chemical vapor deposition
DLE	Digital layer epitaxy
DTA	Differential thermal analysis
FTIR	Fourier transform infrared (spectroscopy)
HTS	High temperature superconductor
IC	Integrated circuit
MBE	Molecular beam epitaxy
MLE	Molecular layer epitaxy
MOCVD	Metal organic chemical vapor deposition
MOD	Metalorganic decomposition
MOSFET	Metal-oxide-semiconductor-field-effect transistors
PECVD	Plasma enhanced chemical vapor deposition
PLD	Pulsed laser deposition
PVD	Physical vapor deposition
RF	Radio frequency
RBS	Rutherford backscattering spectroscopy
rms	root-mean-square
SEM	Scanning electron microscopy
SIMS	Secondary ion mass spectrometry
SNS	Superconductor–normal metal–superconductor
SOFC	Solid oxide fuel cell
TCO	Transparent conducting oxide
TFEL	Thin film electroluminescent
TG	Thermogravimetry
thd	2,2,6,6-Tetramethyl-3,5-heptanedionate
TMP	Trimethylphosphate
TOF-ERDA	Time of flight elastic recoil detection analysis
XPS	X-ray photoelectron spectroscopy
XRD	X-ray diffraction
XRF	X-ray fluorescence
YBCO	Yttrium barium copper oxide, $\text{YBa}_2\text{Cu}_3\text{O}_{7-x}$
YSZ	Ytria-stabilized zirconia

## CONTENTS

1. INTRODUCTION	9
2. GENERAL BACKGROUND	11
2.1 Atomic Layer Epitaxy	11
2.1.1 Principle of the ALE process	11
2.1.2 Benefits and limitations of ALE	13
2.2 Oxide thin films grown by ALE	13
2.3 Literature review of trivalent metal oxide thin films relevant to the present study	15
2.3.1 Binary oxides	15
2.3.2 Ternary oxides	19
3. EXPERIMENTAL	24
3.1 Source materials and substrates	24
3.2 Film deposition	25
3.3 Film characterization	27
4. RESULTS AND DISCUSSION	29
4.1 Binary oxides	29
4.1.1 Film growth and properties	29
4.1.2 Effect of post-annealing on film crystallinity and properties	34
4.2 Ternary oxides	36
4.2.1 Film growth and composition	36
4.2.2 Crystallinity and morphology	40
4.2.3 Effect of post-annealing on film crystallinity and properties	41
5. CONCLUSIONS	47
REFERENCES	49



## 1. INTRODUCTION

High thermal and chemical stability, diamagnetism, and optical transparency are characteristic of many metal oxides. Electrically oxides may be insulating, semiconducting, conducting, or even superconducting. Owing to this wide range of properties, metal oxide thin films are of interest for applications in microelectronics, optics, and optoelectronics as well as in sensors and protective coatings. However, there is still a need to enhance the quality of existing applications and to develop new ones. Either new metal oxide thin films with more suitable properties are required or the quality of the present metal oxide thin films needs to be improved. One way to achieve these aims is through development of new deposition processes.

Atomic layer epitaxy (ALE) is a chemical vapor phase thin film deposition technique patented in the early 1970s in Finland by T. Suntola and J. Antson.<sup>1,2</sup> The unique feature of ALE is that the film growth occurs in a surface-controlled manner, layer by layer.<sup>3-5</sup> In the ALE process for oxide materials, metal and oxygen precursors are alternately pulsed over the substrate surface, with an inert gas pulse or evacuation after each precursor pulse. Thus in ALE, the film growth proceeds *via* alternate surface reactions. An excess of the precursors is supplied to ensure saturation of all the available reactive surface sites, and thus self-limiting growth of the film. ALE offers several attractive features for thin film growth: simple and accurate thickness control, excellent conformality, and good large area uniformity.<sup>4,5</sup> Practice has also shown that ALE-grown thin films often are of superior quality as compared with films made by other methods at corresponding temperatures.<sup>5</sup>

The present thesis provides a summary of work undertaken to grow the binary oxides  $\text{Al}_2\text{O}_3$ ,  $\text{Ga}_2\text{O}_3$ , and  $\text{La}_2\text{O}_3$  and the ternary oxides  $\text{LaNiO}_3$ ,  $\text{LaCoO}_3$ ,  $\text{LaAlO}_3$ , and  $\text{LaGaO}_3$  by the ALE technique.<sup>I-VII</sup> These thin film materials have a variety of existing and potential applications as sensors, catalysts, and optical and protective coatings as well as in micro- and optoelectronics and solid oxide fuel cells. New ALE processes are reported for all of the films studied. Most notably, the feasibility of ALE for producing more complex ternary oxides is demonstrated by extending the use of ALE to perovskite-type oxides.

As the development of an ALE process for ternary compounds often requires knowledge of the growth of the corresponding binary oxides, preliminary studies were undertaken on the

ALE growth of NiO, Co<sub>3</sub>O<sub>4</sub>, Al<sub>2</sub>O<sub>3</sub>, and more detailed studies on the growth of Ga<sub>2</sub>O<sub>3</sub> and La<sub>2</sub>O<sub>3</sub> thin films using  $\beta$ -diketonate metal chelates and ozone as precursors. These studies are reported in Publications II-V. Publications IV and V describe the first experiments on ALE growth of ternary perovskite-type oxides and the growth of LaNiO<sub>3</sub> and LaCoO<sub>3</sub>. The results of these experiments were presented in the doctoral work of Helene Seim as well.<sup>6</sup> Publications VI and VII describe the extension of the work to two other ternary oxides, LaAlO<sub>3</sub> and LaGaO<sub>3</sub>. Furthermore, the growth of another type of mixed oxide, *viz.* phosphorus-doped Al<sub>2</sub>O<sub>3</sub> films from AlCl<sub>3</sub>, water, and either P<sub>2</sub>O<sub>5</sub> or trimethylphosphate is reported in Publication I.

The emphasis in the work now described was on the development of new ALE oxide thin film deposition processes and on the characterization of the resulting thin films for composition, crystallinity, and morphology. Thus, for instance, the electrical properties of the films are not reported even though finding new promising oxide materials for applications in electronics was one of the underlying goals of the research.

## 2. GENERAL BACKGROUND

Chapter 2 is intended to provide the reader with some background with which to evaluate the results obtained in the ALE studies summarized in Chapter 4. The basic principle of the atomic layer epitaxy (ALE) thin film deposition technique is introduced, the benefits and limitations of ALE are discussed, and the metal oxide films already grown by ALE are briefly presented. Previous work on the binary metal oxides  $\text{Al}_2\text{O}_3$ ,  $\text{Ga}_2\text{O}_3$ , and  $\text{La}_2\text{O}_3$  and the ternary metal oxides  $\text{LaNiO}_3$ ,  $\text{LaCoO}_3$ ,  $\text{LaAlO}_3$ , and  $\text{LaGaO}_3$ , the oxides of interest here, is then reviewed. Rather than a comprehensive look at all work done in the area, a summary is offered of the thin film deposition methods employed and the typical film properties obtained. In addition, possible applications of the films are noted.

### 2.1 Atomic layer epitaxy

#### 2.1.1 Principle of the ALE process

The advantageous feature of the atomic layer epitaxy (ALE) technique is the enhanced surface control obtained in thin film growth.<sup>3-5</sup> This is achieved by combining a sequential reactant interaction with a substrate at a temperature that prevents condensation and decomposition of individual reactants on the growing surface. As a general introduction to the ALE process, Figure 1 summarizes the basic ALE reaction cycle leading to the formation of zinc sulfide monolayer from zinc chloride and hydrogen sulphide. In the ideal case, the surface exposed to the precursor is saturated with it *via* chemisorption or by reaction of it with the functional surface groups. The excess of precursor molecules and the released ligands as well as the volatile byproduct molecules are removed from the reactor by a purging step, which leaves behind only the precursor monolayer adsorbed on the substrate surface. The second precursor then reacts with the earlier deposited monolayer, liberating ligands and producing the desired solid layer. The deposition cycle is completed with a second purge step in which the excess precursor and volatile byproduct molecules are removed from the reactor. Thus in ALE, with proper adjustment of the experimental conditions, the film growth proceeds *via* alternate surface reactions and the film growth is self-limiting, *i.e.* the amount of film material deposited during one cycle is determined only by the density of the chemisorption layer or the reaction sites on the

surface.<sup>5</sup> Accordingly, the thickness of the film in an ALE process is determined by the number of deposition cycles.

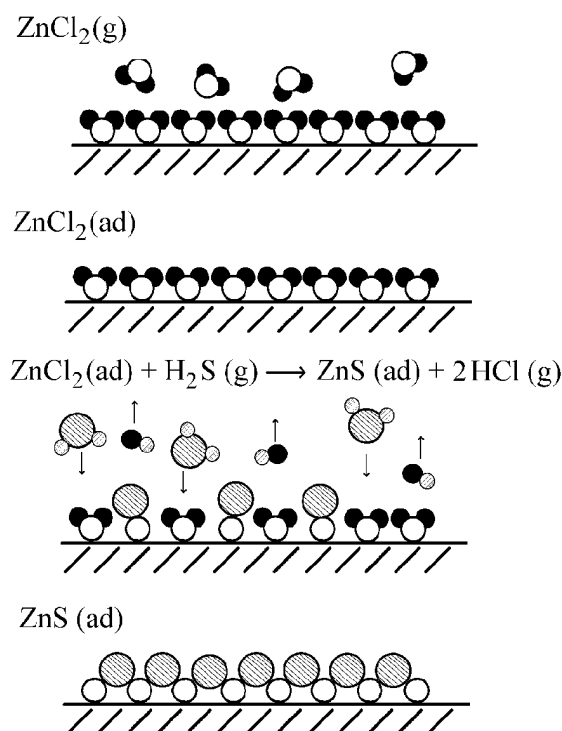


**Figure 1.** A simplified view of an ALE reaction cycle leading to the formation of zinc sulfide thin film from zinc chloride and hydrogen sulphide:  $\text{ZnCl}_2 + \text{H}_2\text{S} \rightarrow \text{ZnS} + 2\text{HCl}$ .<sup>7</sup>

To emphasize the surface control of the reactions taking place upon the previously deposited layer, Dr Suntola coined the term atomic layer epitaxy (ALE), where the word epitaxy comes from Greek and means “on-arrangement”.<sup>3,4</sup> In this meaning, the term ALE covers the deposition of amorphous, polycrystalline and single crystalline thin films. However, the term epitaxy is usually used in a narrower way, to describe the growth of single crystalline layers on a single crystalline surface, which controls the structure of the growing layer. Since this is not the case in most ALE thin film studies, where films are also amorphous and polycrystalline, unfortunate confusions have arisen. Other names have therefore been suggested, such as atomic layer deposition (ALD), atomic layer chemical vapor deposition (ALCVD), atomic layer growth (ALG), digital layer epitaxy (DLE) and molecular layer epitaxy (MLE).<sup>5</sup> Since the late 1990s, the name atomic layer deposition (ALD) appears to have won over the others.<sup>5</sup> In this thesis, only the original name atomic layer epitaxy and the acronym ALE are used.

### 2.1.2 Benefits and limitations of ALE

Compared with other thin film deposition methods, ALE through its inherent surface control offers several attractive features for thin film growth: excellent conformality, simple and accurate thickness control, good large area uniformity, sharp interfaces, good reproducibility, multilayer processing capability, and excellent film qualities at relatively low processing temperatures.<sup>5,8</sup> These advantages combined with the current trend in integrated circuit (IC) manufacturing, *viz.* to decrease device dimensions while increasing aspect ratios, have led to a rapidly growing interest in applying ALE. Currently, ALE is considered one of the most promising substitutes for the techniques already used in the IC industry.<sup>5,9</sup>

A major limitation of ALE is the low deposition rate of the films, since at best one monolayer is deposited during one cycle. Furthermore, in real processes, steric limitations associated with large ligand groups, such as 2,2,6,6-tetramethyl-3,5-heptanedionate (thd) in beta-diketonates, or the limited number of surface groups, for example hydroxyl groups, with which the precursor has to react to become firmly bonded, can lead to a deposition of less than one full monolayer per cycle.<sup>10</sup> As a consequence, even though saturatively formed, the layer contains too few metal atoms, a full monolayer of the thin film material is not formed, and deposition rates are accordingly rather low. However, the thickness required of films has in many cases decreased to the order of a few nanometers so that this drawback of ALE is becoming less important. The lack of good and cost-effective ALE processes for some important materials, such as metals, SiO<sub>2</sub>, and several ternary and multicomponent materials has also restricted the wider use of ALE.<sup>5,9</sup>

## 2.2 Oxide thin films grown by ALE

The ALE process has been used to produce a wide range of thin film materials. The most recent and comprehensive review of ALE deposited films is that of Ritala and Leskelä.<sup>5</sup> Originally, the ALE method was developed to produce luminescent ZnS:Mn and dielectric Al<sub>2</sub>O<sub>3</sub> thin films for electroluminescent (EL) flat panel displays.<sup>1,11</sup> During the 1980s the method was in most cases applied to the growth of polycrystalline and epitaxial III-V and II-VI semiconductor thin films and amorphous insulating aluminum oxide films. In the 1990s ALE was confirmed to be an excellent method for the growth of a variety of oxide films.<sup>5,8,12</sup> As shown in Table 1, however, while the thin film growth of binary metal oxides by ALE has

been demonstrated for several metals and stoichiometries, little work has been done on the more complex ternary compounds.

**Table 1.** ALE-deposited oxide thin films described in the reviews of Ritala and Leskelä<sup>5</sup> and Niinistö *et al.*<sup>12</sup> as well as in the subsequent publications.<sup>13-33</sup>

Dielectric binary oxides	MgO, Al <sub>2</sub> O <sub>3</sub> , <sup>13</sup> Al <sub>2</sub> O <sub>3</sub> :P, SiO <sub>2</sub> , Sc <sub>2</sub> O <sub>3</sub> , <sup>14</sup> Y <sub>2</sub> O <sub>3</sub> , La <sub>2</sub> O <sub>3</sub> , CeO <sub>2</sub> , Nd <sub>2</sub> O <sub>3</sub> , <sup>15</sup> Er <sub>2</sub> O <sub>3</sub> , <sup>16</sup> TiO <sub>2</sub> , <sup>17-22</sup> ZrO <sub>2</sub> , <sup>23-25</sup> HfO <sub>2</sub> , <sup>26</sup> V <sub>2</sub> O <sub>5</sub> , <sup>27</sup> Nb <sub>2</sub> O <sub>5</sub> , Ta <sub>2</sub> O <sub>5</sub> <sup>28,29</sup>
Conductors / semiconductors	WO <sub>3</sub> , MnO <sub>x</sub> , Co <sub>3</sub> O <sub>4</sub> , NiO, ZnO, <sup>30,31</sup> ZnO:Al, <sup>31</sup> ZnO:B, ZnO:Ga, Ga <sub>2</sub> O <sub>3</sub> , In <sub>2</sub> O <sub>3</sub> , In <sub>2</sub> O <sub>3</sub> :Sn, In <sub>2</sub> O <sub>3</sub> :F, SnO <sub>2</sub> , SnO <sub>2</sub> :Sb, Sb <sub>2</sub> O <sub>3</sub>
Ternary oxides	LaNiO <sub>3</sub> , LaCoO <sub>3</sub> , LaMnO <sub>3</sub> , LaAlO <sub>3</sub> , LaGaO <sub>3</sub> , SrTiO <sub>3</sub> , <sup>32</sup> BaTiO <sub>3</sub> , MgAl <sub>2</sub> O <sub>4</sub> Zr <sub>x</sub> Ti <sub>y</sub> O <sub>z</sub> , <sup>33</sup> Bi <sub>x</sub> Ti <sub>y</sub> O <sub>z</sub>
Complex oxides	YBa <sub>2</sub> Cu <sub>3</sub> O <sub>7-x</sub>

In addition to the binary and ternary oxides processed by ALE, an important group of ALE oxides, the nanolaminates, as well as solid solution materials, have recently been attracting attention.<sup>5,10,34-37</sup> A nanolaminate consists of alternating layers of two or more insulator materials so that each separate layer has a thickness ranging from 1 to 20 nm. The goal in depositing nanolaminates has been to improve upon some of the unfavorable properties of single oxide layers while retaining the advantageous properties. The sequential film deposition in ALE makes the preparation of nanolaminates straightforward.<sup>5,10</sup>

ALE has also recently been described in reviews focusing on: ALE precursors,<sup>38</sup> nanotechnology,<sup>10</sup> electronic and optoelectronic materials,<sup>7-9</sup> and catalysts.<sup>39</sup> Although the

advantages of ALE in many cases are obvious, its commercial use has so far been limited to the manufacture of thin film electroluminescent (TFEL) flat panel displays.<sup>3,5,9</sup>

## 2.3 Literature review of trivalent metal oxide thin films relevant to the present study

### 2.3.1 Binary oxides

**Al<sub>2</sub>O<sub>3</sub>.** Alumina (Al<sub>2</sub>O<sub>3</sub>) thin films are characterized by high chemical and thermal stability, high resistivity, relatively high dielectric constant, very low permeability of alkali ions and other impurities, high thermal conductivity, and transparency over a wide range of wavelengths.<sup>40</sup> Owing to these properties, Al<sub>2</sub>O<sub>3</sub> thin films are of interest for applications in microelectronics as well as protective and hard coatings, ion barriers, and optical coatings.<sup>41-45</sup> For more than a decade, the AlCl<sub>3</sub>-H<sub>2</sub>O ALE process has been in industrial use for manufacturing thin film electroluminescent (TFEL) displays, where the Al<sub>2</sub>O<sub>3</sub> film is used as an insulator, passivator and barrier against sodium out-diffusion from the soda lime glass substrate.<sup>3,46</sup> As an alternative gate oxide, alumina has many favorable properties, including a high band gap of ~9 eV, thermodynamic stability with Si at high temperatures, a dielectric constant of ~8-10, and appearance in amorphous phase under the conditions of interest.<sup>41</sup> Different growth methods such as sputtering,<sup>45,47</sup> molecular beam epitaxy (MBE),<sup>48-50</sup> chemical vapor deposition (CVD),<sup>40,51</sup> and atomic layer epitaxy (ALE)<sup>5,13</sup> have been used to produce high-quality aluminum oxide films. The results of CVD and ALE studies are briefly reviewed in the following.

Aluminum chloride [AlCl<sub>3</sub>], trimethyl aluminium [Al(CH<sub>3</sub>)<sub>3</sub>], and various aluminium alkoxides are the most widely used metal precursors in ALE and CVD processing of Al<sub>2</sub>O<sub>3</sub> films, while H<sub>2</sub>O, H<sub>2</sub>O<sub>2</sub>, and N<sub>2</sub>O are the most common oxygen sources.<sup>5,40</sup> The use of aluminum β-diketonates as precursors for ALE growth of Al<sub>2</sub>O<sub>3</sub> has not been reported,<sup>5</sup> but they have been used in several CVD studies.<sup>51-54</sup> Recently, Ritala *et al.*<sup>55</sup> introduced an interesting new ALE process for Al<sub>2</sub>O<sub>3</sub> films where aluminum alkoxide serves as both oxygen and metal source and the film forms when it reacts with another metal compound such as metal chloride or metal alkyl. This process enables the growth of an alumina film on silicon without formation of an interfacial silicon dioxide layer, such as often forms in the conventional ALE processes.

The Al<sub>2</sub>O<sub>3</sub> films deposited by CVD or ALE methods tend to be amorphous because of the relatively low deposition temperatures (<600 °C) employed. A weak tendency towards agglomeration has also been suggested as an explanation for the formation of amorphous films.<sup>56</sup> Typically, Al<sub>2</sub>O<sub>3</sub> film surfaces are smooth, for instance root-mean square roughness values less than 1 nm are reported for 730 nm thick films.<sup>56</sup> The deposition temperature has an effect on film composition, refractive index, and dielectric constant.<sup>57-60</sup> The content of residues (carbon, hydrogen, chlorine) in the films decreases as the deposition temperature is increased, leading to denser film structures, higher refractive indices, and higher dielectric constants.<sup>58-60</sup> The lowest deposition temperature in the MOCVD studies of Al<sub>2</sub>O<sub>3</sub> films was reported in the study of Kim *et al.*,<sup>53</sup> where stoichiometric Al<sub>2</sub>O<sub>3</sub> with a carbon content <2 at.% was obtained at 230 °C with use of Al(acac)<sub>3</sub> and H<sub>2</sub>O as precursors, and also in the plasma enhanced CVD study of Ovsyannikov *et al.*,<sup>51</sup> where highly transparent Al<sub>2</sub>O<sub>3</sub> films were obtained at 200–250 °C with use of Al(acac)<sub>3</sub> and oxygen as reactants. Matero *et al.*<sup>58</sup> have recently reported the growth of very pure Al<sub>2</sub>O<sub>3</sub> films with less than 0.2 at.% of carbon and 1 at.% of hydrogen using the Al(CH<sub>3</sub>)<sub>3</sub>–H<sub>2</sub>O ALE process at 250 °C. Complete elimination of the impurities in ALE-grown Al<sub>2</sub>O<sub>3</sub> films probably requires deposition temperatures higher than 500 °C for AlCl<sub>3</sub>–H<sub>2</sub>O and 400 °C for Al(CH<sub>3</sub>)<sub>3</sub>–H<sub>2</sub>O ALE processes.<sup>60</sup>

Typically the refractive index of ALE-grown Al<sub>2</sub>O<sub>3</sub> film is between 1.65 and 1.70<sup>13,58-60</sup> and a dielectric constant of 7–9 and breakdown field of 3–8 MV/cm are reported.<sup>5,13</sup> Similar results have been obtained in CVD studies.<sup>51</sup>

**Ga<sub>2</sub>O<sub>3</sub>.** Gallium oxide films have been tested during the past ten years or so as materials for oxygen<sup>61,62</sup> and reducing gas<sup>63-65</sup> sensors. Recently, Ga<sub>2</sub>O<sub>3</sub> sensors for detecting ethanol, carbon monoxide, and methane gases have been commercialized.<sup>66</sup> Doped gallium oxide films have attracted interest as emitting layers for use in thin film electroluminescent (TFEL) devices.<sup>67-69</sup> Dielectric films composed of Ga<sub>2</sub>O<sub>3</sub> and Gd<sub>2</sub>O<sub>3</sub>, for example, have been shown to effectively passivate GaAs surfaces in the preparation of metal-oxide-semiconductor-field-effect transistors (MOSFET).<sup>70-72</sup> In addition, gallium oxide films have been investigated for an application as transparent conducting oxide (TCO) in optoelectronics.<sup>73</sup>



Most of the gallium oxide films have been deposited by physical vapor deposition (PVD) methods such as RF magnetron sputtering,<sup>74-78</sup> electron beam evaporation,<sup>79,80</sup> vapor evaporation,<sup>81</sup> and pulsed-laser deposition (PLD).<sup>73</sup> Although CVD methods are probably the most practical way to prepare thin films for large-scale applications, the first articles describing the CVD growth of Ga<sub>2</sub>O<sub>3</sub> films were published as late as 1996<sup>82</sup> and after that only three reports on CVD growth of Ga<sub>2</sub>O<sub>3</sub> films<sup>83-85</sup> have appeared in the literature. In addition, spray pyrolysis has been attempted.<sup>86,87</sup>

The precursors used in CVD studies are gallium acetylacetonate [Ga(acac)<sub>3</sub>],<sup>82</sup> gallium tris-hexafluoroacetylacetonate [Ga(hfac)<sub>3</sub>],<sup>82</sup> anhydrous gallium nitrate [NO<sub>2</sub>Ga(NO<sub>3</sub>)<sub>4</sub>],<sup>85</sup> a gallium dimethylamide complex [Ga(OCH(CF<sub>3</sub>)<sub>2</sub>)<sub>3</sub>(NHMe<sub>2</sub>)],<sup>84</sup> and a gallium alkoxide complex [Ga(μ-O-t-Bu)(O-t-Bu)<sub>2</sub>]<sub>2</sub>,<sup>83</sup> while ozone, oxygen, and air are used as oxygen sources. Although relatively low deposition temperatures between 250 and 700 °C were used in the CVD studies the films were fairly pure, for instance the residual carbon content was typically below 3 at-%. However, some of the films contained an excess of oxygen,<sup>83-85</sup> which increased at lower deposition temperatures.<sup>83,84</sup>

Gallium oxide can adopt several crystalline phases, such as α, β, γ, σ, and ε, of which the high-temperature monoclinic β-Ga<sub>2</sub>O<sub>3</sub> modification is the most stable and is also preserved upon cooling. In general, Ga<sub>2</sub>O<sub>3</sub> films are amorphous when deposited below 850 °C, whereas polycrystalline, monoclinic β-Ga<sub>2</sub>O<sub>3</sub> phase is formed when the films are deposited or annealed at temperatures between 850 and 1100.<sup>81-83,86</sup> There is one notable exception: polycrystalline β-type Ga<sub>2</sub>O<sub>3</sub> was obtained when gallium oxide films were grown at 350 °C by spray pyrolysis.<sup>87</sup> This temperature is surprisingly low relative to the values reported in other studies and has not been confirmed by other groups.

Gallium oxide films are highly transparent in the 350–1100 nm region and the refractive index of stoichiometric films is 1.88–1.94.<sup>79,82-84</sup> The reported band gap is in the range of 4.4–5.1 eV.<sup>73,80,81,83,84,86</sup> Stoichiometric gallium oxide is insulating at room temperature but becomes an *n*-type semiconductor when slightly oxygen deficient. Oxygen deficiency in the crystal lattice is produced at high temperatures or by the use of low oxygen partial pressure during the growth process. Doping of gallium oxide films with tin has also been reported to

result in *n*-type semiconductivity.<sup>73</sup> The dielectric constant in Ga<sub>2</sub>O<sub>3</sub> films<sup>80</sup> and single crystals<sup>88</sup> is 10, while resistivity is in the order 10<sup>12</sup>-10<sup>13</sup> Ωcm at room temperature.<sup>79,80</sup>

**La<sub>2</sub>O<sub>3</sub>.** Although La<sub>2</sub>O<sub>3</sub> thin films have a large number of potential applications, very few studies on their preparation and especially on their characterization have been carried out. La<sub>2</sub>O<sub>3</sub> films have been deposited by different evaporation methods,<sup>89-94</sup> by CVD,<sup>95,96</sup> and by pyrolysis techniques.<sup>97-99</sup> A conventional CVD preparation<sup>95</sup> of La<sub>2</sub>O<sub>3</sub> films from La(thd)<sub>3</sub> and water at 570 °C resulted in poorly crystalline, pale brown films, whereas nearly stoichiometric La<sub>2</sub>O<sub>3</sub> films with a carbon contamination of 1.6 wt.-% were obtained from the same precursors at 400 °C using the plasma enhanced CVD (PECVD) process.<sup>96</sup>

Lanthanum oxide films deposited below ~600 °C are usually amorphous, whereas the polycrystalline, hexagonal phase is obtained when the films are deposited or annealed at higher temperatures. However, the recent study of Wang *et al.*<sup>99</sup> reports the growth of monoclinic La<sub>2</sub>O<sub>3</sub> films by spray pyrolysis method at 550 °C. This is somewhat surprising, since the monoclinic structure has not previously been reported for lanthanum oxide.<sup>100, 101</sup> Cubic (low temperature modification) La<sub>2</sub>O<sub>3</sub> phase is reported<sup>100,101</sup> to exist below ~400 °C, while hexagonal (low temperature modification) La<sub>2</sub>O<sub>3</sub> exists between ~400 and 2040 °C. However, the cubic La<sub>2</sub>O<sub>3</sub> is probably metastable.<sup>100,101</sup>

Lanthanum oxide films are transparent over a wide wavelength range from UV to near-IR.<sup>92,96,98</sup> The refractive index is reported<sup>92</sup> to be 1.85 and the band gap is about 4 eV.<sup>41</sup> The most recent reports on La<sub>2</sub>O<sub>3</sub> thin films focus on their use as gate dielectric<sup>94,102,103</sup> or study the interaction between La<sub>2</sub>O<sub>3</sub> and silicon substrate.<sup>104,105</sup> Excellent results have been obtained for Al/La<sub>2</sub>O<sub>3</sub>/Si capacitor structures formed by the evaporation of La onto Si, followed by low-temperature thermal oxidation and *ex situ* Al gate deposition.<sup>102,103</sup> A physical thickness of 33 Å La<sub>2</sub>O<sub>3</sub> with a dielectric constant of 27 gave an equivalent oxide thickness of 4.8 Å, high breakdown field of 13.5 MV/cm, and leakage current density of 0.06 A/cm<sup>2</sup> at 1.0 V. However, the usefulness of La<sub>2</sub>O<sub>3</sub> as a gate dielectric may require further examination, since in recent studies silicon has been shown to diffuse into the La<sub>2</sub>O<sub>3</sub> film forming an interfacial SiO<sub>2</sub> or silicate layer<sup>94,104,105</sup> It has even been found to diffuse through the lanthanum oxide film.<sup>94,104</sup> Another factor to be considered is the tendency of La<sub>2</sub>O<sub>3</sub> to absorb water vapor and carbon dioxide from air, so that any *ex situ* exposure of these films to air will result in an uncontrolled reaction and stoichiometry.<sup>41</sup>

### 2.3.2 Ternary oxides

**LaNiO<sub>3</sub>.** LaNiO<sub>3</sub> is one of the few conductive oxides with a crystal structure suitable for integration in epitaxial heterostructures with perovskites of enormous technological potential such as colossal magnetoresistance (CMR) materials,<sup>106</sup> high-temperature superconductors (HTS),<sup>107-109</sup> and ferroelectrics.<sup>110-115</sup> LaNiO<sub>3</sub> has a rhombohedrally distorted perovskite structure with a pseudocubic lattice parameter of 3.84 Å, which matches well with the unit cells of common superconductors [YBa<sub>2</sub>Cu<sub>3</sub>O<sub>7-x</sub> (YBCO) and Tl-oxide based superconductors] as well as those of ferroelectrics [PbTiO<sub>3</sub> (PT) and PbZr<sub>x</sub>Ti<sub>1-x</sub>O<sub>3</sub> (PZT), BaTiO<sub>3</sub> (BT) and BaSr<sub>x</sub>Ti<sub>1-x</sub>O<sub>3</sub> (BST)], allowing epitaxial growth of these perovskites on LaNiO<sub>3</sub> substrate. In addition, LaNiO<sub>3</sub> is conductive with an electrical resistivity of only a few hundred μΩ cm at room temperature and exhibits metallic-like temperature dependence. Most studies in the literature report the use of LaNiO<sub>3</sub> films in heterostructures with other perovskites designed for use as electrodes in ferroelectric capacitors,<sup>110-115</sup> as buffer layers or substrates for YBCO,<sup>107</sup> or as metallic parts in superconductor–normal metal–superconductor (SNS) junctions.<sup>108,109</sup> Recently, LaNiO<sub>3</sub> was found to be a promising material to replace Pt electrodes on silicon substrates.<sup>115-117</sup>

LaNiO<sub>3</sub> thin films have been deposited by physical vapour deposition methods such as molecular beam epitaxy (MBE),<sup>118</sup> pulsed laser deposition (PLD),<sup>119-124</sup> RF magnetron sputtering,<sup>125-127</sup> spin-coating,<sup>128</sup> spray combustion flame<sup>129</sup> and spray-pyrolysis,<sup>106</sup> and sol-gel<sup>130-132</sup> and metalorganic decomposition (MOD)<sup>133,134</sup> techniques. However, only the Gorbenko group,<sup>135,136</sup> has reported the growth of LaNiO<sub>3</sub> thin films by a modified CVD process called flash powder evaporation. The film deposition at 750–850 °C on MgO(100) and LaAlO<sub>3</sub>(100) substrates using La(thd)<sub>3</sub>, Ni(thd)<sub>2</sub> or Ni(acim)<sub>2</sub>, and oxygen as precursor resulted in stoichiometric and smooth LaNiO<sub>3</sub> films with a cubic (100) oriented crystal structure. The films were metallic with a room temperature resistivity of 460 μΩ cm.

Most of the LaNiO<sub>3</sub> films are amorphous when deposited below temperatures of 400–600 °C but crystallize in cubic<sup>124,129,133,135</sup> or rhombohedral<sup>108,127</sup> forms when grown or post-annealed at higher temperatures. The films deposited by RF magnetron sputtering seem to be an exception, since they are crystalline at temperatures below 400 °C and even at temperatures as low as 150–250 °C.<sup>126,127</sup> The substrate has a notable influence on the film growth.

Irrespective of the deposition technique, the films deposited on lattice-matched substrates, such as single-crystal  $\text{LaAlO}_3(100)$  and  $\text{SrTiO}_3(100)$ , are highly epitaxial and smooth,<sup>118-122,128,130</sup> while the films deposited on  $\text{Si}(100)$  are either randomly oriented<sup>123,131</sup> or at best highly oriented but polycrystalline.<sup>126,127,133</sup> Both (100) and (110) orientations on  $\text{Si}(100)$  are observed.<sup>126,127,133</sup> In addition, (100) oriented, textured growth is obtained on  $\text{YSZ}(100)$ <sup>122</sup> and  $\text{MgO}(100)$ <sup>129,135</sup> substrates as well as on  $\text{Pt}$ <sup>117,127</sup> and textured  $\text{Ni}$ .<sup>125</sup> The films grown on sapphire, quartz, or glass substrates are polycrystalline.<sup>128,129</sup> Sánchez *et al.*<sup>124</sup> recently reported the growth of epitaxial  $\text{LaNiO}_3$  thin films on  $\text{Si}(100)$  by using an intermediate double layer consisting of a  $\text{CeO}_2/\text{YSZ}$  structure as a buffer layer.

Most of the  $\text{LaNiO}_3$  films have a smooth and crack-free surface with a surface roughness of below 2 nm.<sup>119,123,124,130</sup> The films have good metallic properties and a room temperature resistivity of 150-500  $\mu\Omega$  cm is widely reported for epitaxial  $\text{LaNiO}_3$  films. The resistivity in polycrystalline  $\text{LaNiO}_3$  films is higher, 600–2600  $\mu\Omega$  cm. The lowest resistivity reported, 50  $\mu\Omega$  cm, is found in films deposited on  $\text{SrTiO}_3(100)$  by a PVD method.<sup>120</sup>

**LaCoO<sub>3</sub>.** The growth of  $\text{LaCoO}_3$  thin films by CVD methods does not seem to have been attempted and only a few reports describe the deposition of films by sputtering,<sup>137,138</sup> sol-gel,<sup>139,140</sup> spin-coating,<sup>141</sup> spray pyrolysis<sup>142</sup> and spray combustion flame<sup>129</sup> and electrochemical oxidation<sup>143</sup> techniques. The  $\text{LaCoO}_3$  films deposited below 500 °C are amorphous but become crystalline when deposited or annealed above this temperature. Most of the films are polycrystalline, probably because of the deposition on non-lattice-matched substrates such as glass, Si, sapphire, alumina, and YSZ. However, highly (100) oriented  $\text{LaCoO}_3$  films were obtained on  $\text{MgO}(100)$  substrates by Ichinose *et al.*<sup>129</sup> In polycrystalline bulk form,  $\text{LaCoO}_3$  is reported to have a rhombohedrally distorted perovskite-type structure with a pseudocubic lattice parameter of 3.81 Å. Both cubic<sup>129,137-139,142</sup> and rhombohedral<sup>129,141</sup> crystal structures have been reported in thin film form.

Electrical resistivity of 0.5–1  $\Omega\text{cm}$ <sup>137,142,144</sup> is reported for  $\text{LaCoO}_3$  films at room temperature, while at high temperatures they show metallic-like conduction behavior and a resistivity comparable to that of metals.<sup>137</sup> Doping the La-site of  $\text{LaCoO}_3$  with strontium modifies the electrical properties of the films and, for instance, the room temperature resistivity of

$\text{La}_{1-x}\text{Sr}_x\text{CoO}_3$  films is reduced down to the range of 200–1500  $\mu\Omega\text{ cm}$ .<sup>144,145</sup> The potential applications of  $\text{LaCoO}_3$  and  $\text{La}_{1-x}\text{Sr}_x\text{CoO}_3$  films include gas<sup>138</sup> and ion<sup>146</sup> sensors, electrodes in ferroelectric capacitors,<sup>144,145</sup> and materials for high temperature solid oxide fuel cells (SOFC).

**LaAlO<sub>3</sub>.** Lanthanum aluminate has an ideal cubic perovskite structure at temperatures higher than ~530 °C, but below that it transforms into a rhombohedral form. The rhombohedral distortion is slight (0.2%), though, and therefore the phase is generally viewed as pseudocubic with a lattice constant of 3.79 Å.<sup>147</sup> With its matching lattice parameters and chemical compatibility,  $\text{LaAlO}_3$  is a promising material for use as a buffer layer for epitaxial growth of perovskite-type films such as HTS, ferroelectrics, and CMR oxides. Its dielectric properties, for example, reasonably low dielectric constant of 24 and low dielectric loss tangent,<sup>148,149</sup> make it a suitable material for many applications as well. Most often,  $\text{LaAlO}_3$  has been investigated for use as a buffer layer<sup>150-152</sup> or substrate<sup>153</sup> for HTS films. A novel modification is to grow  $\text{LaAlO}_3$  film on biaxially textured and flexible Ni metal tapes to be employed as a buffer layer for HTS films.<sup>154,155</sup> Potential applications of these structures are power transmission lines, electric generators, and high-field magnets.<sup>154</sup>

$\text{LaAlO}_3$  thin films have been deposited on a variety of substrates by metalorganic chemical vapor deposition (MOCVD),<sup>156-160</sup> pulsed laser deposition,<sup>154,161</sup> RF magnetron sputtering,<sup>151,162-164</sup> sol-gel process,<sup>155,165-167</sup> spray pyrolysis,<sup>142</sup> and spray combustion flame technique.<sup>129</sup> Typically, solutions of metal thd or acac chelates are used as precursors in the CVD studies, but in the study of Malandrino *et al.*<sup>159</sup> a novel lanthanum precursor,  $\text{La}(\text{hfa})_3 \cdot \text{diglyme}$ , was introduced.

Both the substrate and the growth temperature have a marked influence on the crystallinity of the films. Irrespective of the deposition method, epitaxial  $\text{LaAlO}_3$  films are obtained on perovskite substrates ( $\text{SrTiO}_3$ ,  $\text{NdGaO}_3$ , and  $\text{LaAlO}_3$ ), while amorphous or polycrystalline films are obtained on Si,  $\text{SiO}_2$ ,  $\text{MgO}$ ,  $\text{Al}_2\text{O}_3$ ,  $\text{CeO}_2$  or YSZ substrates under similar conditions.<sup>144,154,156,166</sup> As a rule, the deposition temperatures needed to obtain crystalline  $\text{LaAlO}_3$  films are higher than 800–900 °C for films deposited on perovskite substrates and around 1000 °C for films grown on other substrates. Other deposition conditions than growth temperature may also have an effect, since highly (111) and (100) oriented  $\text{LaAlO}_3$  films have been obtained on YSZ(100) and

MgO(100) at 1000–1050 °C with use of thermal MOCVD and volatile surfactant-assisted MOCVD, respectively.<sup>156,158</sup> These recent studies introduce a novel approach to the CVD growth of LaAlO<sub>3</sub> films, namely the use of liquid single source<sup>158</sup> or film growth in the presence of a volatile low melting point oxide.<sup>156</sup> The crystalline quality of the LaAlO<sub>3</sub> films has clearly improved as a result.

Experiments on LaAlO<sub>3</sub> thin film growth on silicon show that interdiffusion between LaAlO<sub>3</sub> and Si cannot be ruled out. It seems that, at lower temperatures than 850–900 °C, polycrystalline or even oriented LaAlO<sub>3</sub> films can be grown on silicon,<sup>151,162,163</sup> but at deposition or annealing temperatures over 900 °C, solid-state reactions between silicon and LaAlO<sub>3</sub> film are initiated.<sup>159-161</sup> These are evident in XRD patterns where crystalline phases such as La<sub>2</sub>Si<sub>2</sub>O<sub>7</sub>, La-Si, Al<sub>2</sub>O<sub>3</sub>, Al-Si-O and La-Al-Si-O are reported.<sup>159-161</sup> Unfortunately, the mixing of silicon and LaAlO<sub>3</sub> has been identified only by XRD, while the element depth distributions and film–substrate interfaces have not been characterized, making the conclusions uncertain.

**LaGaO<sub>3</sub>.** Many of the studies concerning LaGaO<sub>3</sub> have been motivated by its possible use as a substrate for epitaxial growth of high-temperature superconducting (HTS) films. At room temperature LaGaO<sub>3</sub> in bulk form has an orthorhombically distorted perovskite-type structure with a pseudocubic lattice parameter of 3.89 Å. The lattice and thermal-expansion match of LaGaO<sub>3</sub> with HTS materials is good and its dielectric constant at room temperature ( $\epsilon=25$ ) is significantly lower than that of the commonly used SrTiO<sub>3</sub> substrate ( $\epsilon=277$ ).<sup>153,168</sup> However, a first-order phase transition of LaGaO<sub>3</sub> at ~150 °C, from orthorhombic to rhombohedral form,<sup>169,170</sup> is reported to cause surface roughening, which can be detrimental to the properties of very thin or patterned HTS films.<sup>171</sup> LaGaO<sub>3</sub> can be characterized as a mixed electronic–ionic conductor. Doping the La-site with Sr and the Ga-site with Mg greatly enhances its ionic conductivity. This doubly doped LaGaO<sub>3</sub> has been described as a superior oxide ion conductor with a high ionic conductivity at elevated temperatures.<sup>172</sup> Mixed electronic–ionic conductors have applications in air-separating membranes, electrodes, and gas sensors. Doped LaGaO<sub>3</sub> has also been examined for use as an electrolyte in solid oxide fuel cells (SOFC).<sup>172</sup>

Only three reports were found in the literature dealing with the thin film growth of LaGaO<sub>3</sub>. As in the case of other perovskite-type oxides, the substrate employed seems to have a significant

effect on film crystallinity. Epitaxial LaGaO<sub>3</sub> film was obtained on single-crystal LaAlO<sub>3</sub>(100) substrate with use of a sol-gel process<sup>173</sup> followed by post-annealing at 850 °C, whereas LaGaO<sub>3</sub> films deposited on sapphire (110) and sapphire (001) at 900 °C by a spray-ICP technique<sup>174</sup> were (112) and (022) oriented, respectively. Furthermore, randomly oriented LaGaO<sub>3</sub> films were obtained on silicon (111) after films deposited by RF magnetron sputtering<sup>151</sup> were annealed at 900 °C for 30 minutes. It appears that LaGaO<sub>3</sub> thin films have not been deposited by chemical vapor deposition (CVD) methods, making the ALE study reported in the present work the first of its kind.

### 3. EXPERIMENTAL

The main experimental features are briefly presented in this section. For details of the experiments, see publications I-VII.

#### 3.1 Source materials and substrates

The source materials and substrates are listed in Table 2.

**Table 2.** Source materials and substrates.

Film	Source materials	Substrates
Al <sub>2</sub> O <sub>3</sub> :P	AlCl <sub>3</sub> (>98%, Merck), H <sub>2</sub> O P <sub>2</sub> O <sub>5</sub> (granusic 99%, J.T. Baker), trimethylphosphate (TMP, >97%, Merck)	Soda lime glass, Si(100), Au-covered glass
Ga <sub>2</sub> O <sub>3</sub>	Ga(acac) <sub>3</sub> , H <sub>2</sub> O, O <sub>2</sub> , O <sub>3</sub>	Soda lime and Corning glass, Si(100)
La <sub>2</sub> O <sub>3</sub>	La(thd) <sub>3</sub> , O <sub>3</sub>	Soda lime glass, Si(100)
LaNiO <sub>3</sub>	La(thd) <sub>3</sub> , Ni(thd) <sub>2</sub> , O <sub>3</sub>	Corning glass
LaCoO <sub>3</sub>	La(thd) <sub>3</sub> , Co(thd) <sub>2</sub> , O <sub>3</sub>	Soda lime and Corning glass
LaAlO <sub>3</sub>	La(thd) <sub>3</sub> , Al(acac) <sub>3</sub> , O <sub>3</sub>	Soda lime glass, Si(100), MgO-buffered Si(100), sapphire, SrTiO <sub>3</sub> (100)
LaGaO <sub>3</sub>	La(thd) <sub>3</sub> , Ga(acac) <sub>3</sub> , O <sub>3</sub>	Soda lime glass, Si(100), MgO-buffered Si(100), sapphire, MgO(100), SrTiO <sub>3</sub> (100), LaAlO <sub>3</sub> (100)

The metal beta-diketonates were synthesized by methods described in the literature.<sup>175,176</sup> The synthesis consisted of precipitation with metal nitrates or chlorides in aqueous ethanolic solution of alkali(thd) or alkali(acac). The complexes that formed were separated by filtration, the powder was dried in vacuum at 50 °C, and the final purification was carried out by vacuum sublimation. The molecular structures of the metal beta-diketonates are presented in Fig. 2. The stability and volatility of the synthesized source materials were studied by simultaneous thermogravimetric (TG) and differential thermal analysis (DTA) measurements.<sup>II,IV</sup> A pressure of 1-3 mbar and nitrogen atmosphere were chosen to simulate



the growth conditions inside the ALE reactor. Ozone was generated from oxygen gas in an ozone generator.

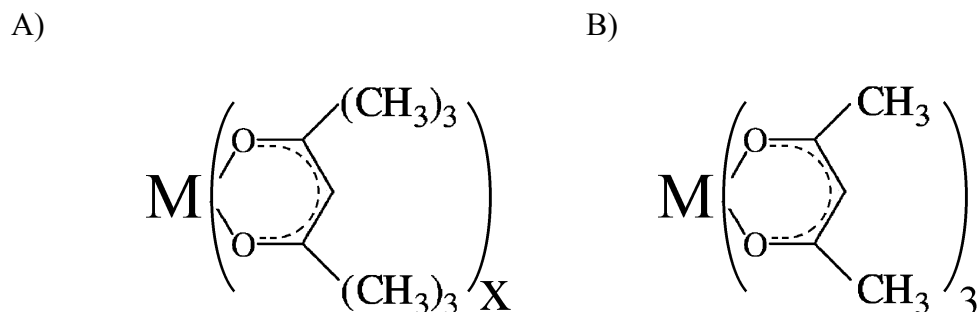


**Figure 2.** Molecular structures of metal beta-diketonates. A)  $M(\text{thd})_x$ , where  $M = \text{La}$  ( $x=3$ ),  $\text{Ni}$ , or  $\text{Co}$  ( $x=2$ ), B)  $M(\text{acac})_3$ , where  $M = \text{Al}$  or  $\text{Ga}$ .

All Si(100) substrates that were used were covered with the native oxide. In the case of phosphorus-doped  $\text{Al}_2\text{O}_3$  films, thermally oxidized Si(100) covered with a 170 nm thick oxide layer was used as substrate. Before use the glass substrates were cleaned ultrasonically in ethanol and deionized water and carefully blown to dryness with nitrogen. The other substrates that were used were only rinsed with ethanol and deionized water and blown dry with nitrogen.

### 3.2 Film deposition

The thin film depositions were carried out in three different flow-type, hot-wall ALE reactors. A traveling-wave-type commercial F-120 reactor (ASM Microchemistry Ltd) operated under a pressure of 10 mbar was used in a study I. In this reactor two substrates are located face to face with a distance of only 2 mm between. A detailed description of the reactor can be found in Ref. 5. A prototype flow-tube-type reactor described in detail in the patent literature<sup>177</sup> was used in studies II, IV, and V, while a commercial F-120 flow-tube-type reactor manufactured by ASM Microchemistry Ltd (Espoo, Finland) was used in studies III, VI, and VII. The difference between these two flow-tube-type reactors is mainly in the dimensions of the tubular (active) reactor chamber. The pressure in these reactors during deposition was 1–3 mbar. A schematic drawing of the flow-tube-type ALE reactor is shown in Fig. 3. In all three

reactors, nitrogen (>99.999%) obtained from a cylinder or a nitrogen generator served both as carrier and purging gas.

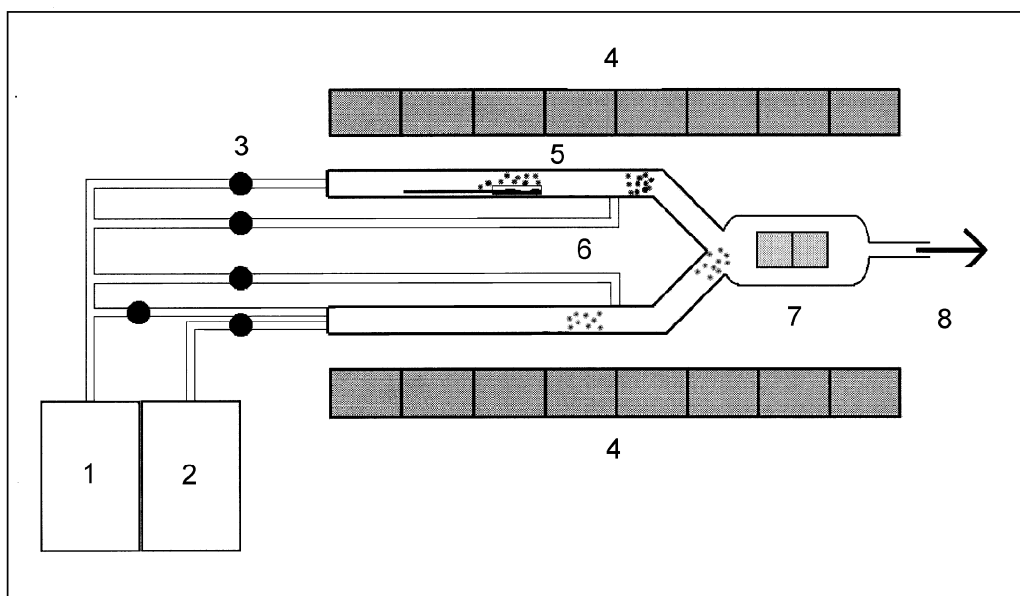


**Figure 3.** Schematic drawing of the flow-tube-type ALE reactor.<sup>7</sup> (1) N<sub>2</sub> generator, (2) O<sub>3</sub> generator or temperature-controlled vessel for water, (3) pulsing valves, (4) heating elements, (5) source boat for solid precursor, (6) inlets for purge gas (N<sub>2</sub>), (7) tubular reactor chamber with substrates, (8) outlet to vacuum pump.

The solid precursors were evaporated inside the reactor from open glass boats held at the temperature chosen for the precursor in question. The furnace temperature and inert gas valving controlled their pulsing and dosage. This approach was also used with liquid TMP. Water was contained in a vessel held in a thermostated bath outside the reactor and was introduced to the reactor through a capillary by means of its own vapor pressure. A solenoid valve in the supply line and inert gas valving inside the reactor accomplished the pulsing of water. The water flow was controlled by a needle valve located in front of the solenoid valve. Ozone pulsing and dosage was controlled in a similar way. Typically, four substrates of size 5 x 5 cm<sup>2</sup> were vertically loaded inside the flow-tube-type reactor chamber in a back-to-back configuration (see Fig. 3). Substrates of smaller size were mounted on a special substrate holder.

### 3.3 Film characterization

The analytical techniques used for the characterization of thin films are summarized in Table 3. More detailed information about the instrumentation and the measurements can be found in the experimental sections of Publications I-VII.

**Table 3.** Analytical techniques used in the characterization of thin films.

Information	Technique
Thickness	Spectrophotometry, profilometry, RBS
Refractive index	Spectrophotometry
Elemental composition	RBS, TOF-ERDA, XRF, XPS
Crystallinity	XRD
Morphology	AFM, SEM
Elemental depth distribution	SIMS, RBS, TOF-ERDA, (XPS)
Structure & identification	FTIR, XRD
Density	RBS
Resistivity	Four-point probe
Electronic state of nickel	Magnetic susceptibility

Thicknesses and refractive indices of the films were determined by fitting the transmittance and reflectance spectra<sup>178</sup> measured in the region 190-1100 nm for silicon and 370-1000 nm for glass substrates.<sup>I-III,VI,VII</sup> The thicknesses of non-transparent films on glass substrates were measured with a profilometer,<sup>IV,V</sup> which was also used to verify some of the results obtained by optical UV-Vis spectroscopy.<sup>I,III</sup> The thicknesses in units  $\text{at}/\text{cm}^2$  obtained by RBS together with thicknesses determined by spectroscopy were used to estimate the density of the films.<sup>I,III</sup> Typically, the thickness of deposited films was between 50 and 400 nm.

Film composition and stoichiometry were determined by Rutherford backscattering spectrometry (RBS)<sup>I-III,V-VII</sup> and time-of-flight elastic recoil spectrometry (TOF-ERD).<sup>III,VI,VII</sup> Both techniques yielded information about the content and depth distribution of the main components in the films. The heavier elements and impurity contents are readily determined from the RBS spectra, while the amounts of oxygen and lighter impurities such as carbon and hydrogen can more accurately be obtained by TOF-ERD analysis. The uncertainties of the

TOF-ERD and RBS measurements are below 0.1 at.% units for contents below 1 at.% and below 0.2 at.% for contents above 1 at.%. In addition, X-ray fluorescence (XRF) spectrometry was used in elemental analysis.<sup>I,VI,VII</sup> XRF is a rapid and non-destructive method, which after proper calibration by RBS can be used in a routine way<sup>I,VI,VII</sup> for the determination of film composition.

The elemental depth distributions were also measured by secondary ion mass spectrometry (SIMS).<sup>VII</sup> The XPS measurements were done without sputtering so that only the surface composition of the films was characterized.<sup>IV-VII</sup> Structural information about the films was obtained from Fourier transform infrared (FTIR) spectra.<sup>I,III,VI</sup> FTIR is a convenient method for surface analysis since it does not destroy the sample and no special conditions such as ultra high vacuum are required for the measurement. In the present studies both FTIR transmission spectroscopy (films deposited on silicon) and reflection spectroscopy (films deposited on gold layer) were applied.

The film crystallinity was determined by X-ray diffraction (XRD),<sup>II-VII</sup> while information about the epitaxial quality of the films was obtained by rocking curve measurements.<sup>VI,VII</sup> The surface quality and morphology of the films were examined by atomic force microscopy (AFM)<sup>III,IV,VI,VII</sup> and scanning electron microscopy (SEM).<sup>IV</sup>

The electrical resistivity of the LaNiO<sub>3</sub> films was measured by the four-point probe method and the electronic state of nickel in the films was determined by magnetic susceptibility studies.<sup>IV</sup>

## 4. RESULTS AND DISCUSSION

This chapter summarizes the results of ALE thin film depositions of the binary oxides  $\text{La}_2\text{O}_3$  and  $\text{Ga}_2\text{O}_3$  and the ternary oxides  $\text{LaNiO}_3$ ,  $\text{LaCoO}_3$ ,  $\text{LaAlO}_3$ , and  $\text{LaGaO}_3$ . In addition, the preliminary results of studies on  $\text{NiO}$ ,  $\text{Co}_3\text{O}_4$ , and  $\text{Al}_2\text{O}_3$  films and some unpublished results concerning the properties of phosphorus-doped  $\text{Al}_2\text{O}_3$  thin films are included in section 4.1.1.

### 4.1 Binary oxides

#### 4.1.1 Film growth and properties

$\text{La}_2\text{O}_3$ .<sup>III</sup> A temperature-independent, self-limited growth, with a growth rate of  $0.36 \text{ \AA}/\text{cycle}$  on both silicon and soda lime glass substrates, was obtained between  $225$  and  $275 \text{ }^\circ\text{C}$ . Between  $275$  and  $425 \text{ }^\circ\text{C}$  the growth rate increased with temperature, and above  $425 \text{ }^\circ\text{C}$  the films became profiled and the deposition was no longer controllable, indicating decomposition of the  $\text{La}(\text{thd})_3$  precursor. The thickness of the films deposited at  $250$ ,  $350$ , and  $375 \text{ }^\circ\text{C}$  showed a linear relation with the number of deposition cycles and the growth rates at the mentioned temperatures were independent of the  $\text{La}(\text{thd})_3$  pulse duration, indicating that surface controlled growth was achieved even at temperatures up to  $375 \text{ }^\circ\text{C}$ . All the films deposited between  $225$  and  $425 \text{ }^\circ\text{C}$  exhibited good thickness uniformity over the substrate area of  $10 \times 5 \text{ cm}^2$ . The increase in the growth rate at higher deposition temperatures is most likely due to partial decomposition of the  $\text{La}(\text{thd})_3$  precursor. The  $\text{La}(\text{thd})_3$  may lose one or two of its three ligands either in the gas phase or upon adsorption on the film surface, with the result that the density of surface coverage by the precursor is enhanced and the growth rate increased, but the surface-controlled growth mode is maintained. A similar phenomenon was recently detected in the ALE growth of  $\text{Y}_2\text{O}_3$  thin films.<sup>179</sup>

The composition of the films changed with temperature. RBS and TOF-ERD analysis showed that the films grown between  $225$  and  $275 \text{ }^\circ\text{C}$  consisted of  $\text{La}_2\text{O}_2\text{CO}_3$ , whereas between  $300$  and  $325 \text{ }^\circ\text{C}$  a phase mixture of  $\text{La}_2\text{O}_3$  and  $\text{La}_2\text{O}_2\text{CO}_3$  was likely formed. This was further confirmed by XRD results, which showed that the films grown below  $300 \text{ }^\circ\text{C}$  were amorphous and those grown above  $300 \text{ }^\circ\text{C}$  were cubic, polycrystalline  $\text{La}_2\text{O}_3$ . At  $350 \text{ }^\circ\text{C}$  and above, the films contained cubic  $\text{La}_2\text{O}_3$ ; however, they contained an excess of oxygen, which could be

explained in terms of the carbonate-type impurity seen in the FTIR spectra of the films (Fig. 4a). The  $\text{La}_2\text{O}_3$  films deposited in the temperature range of 375–425 °C contained about 3 at.% of carbon, which is less than the carbon content in films grown by CVD methods.<sup>96</sup> The cubic  $\text{La}_2\text{O}_3$  phase is regarded as metastable in the bulk form<sup>100</sup> but nevertheless was observed to be the only crystalline phase in the as-deposited films. A similar phenomenon has been observed earlier in the ALE-grown  $\text{La}_2\text{S}_3$  films, which crystallized in cubic form at 450-500 °C, although the bulk  $\text{La}_2\text{S}_3$  is reported to be stable only at 1000 °C or above.<sup>180</sup>

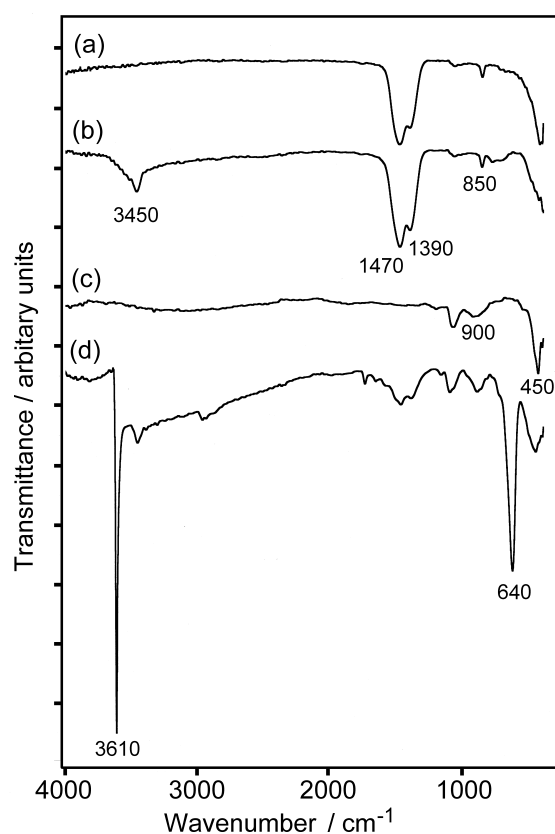


**Figure 4.** FTIR spectra of as-grown cubic  $\text{La}_2\text{O}_3$  film deposited at 350 °C on silicon substrate (a) and of the same film after storage of a few weeks (b). FTIR spectra of a hexagonal  $\text{La}_2\text{O}_3$  film heat-treated at 800 °C in nitrogen atmosphere for 30 minutes (c) and after exposure to air (d).<sup>III</sup>

FTIR was found to be a convenient method to obtain qualitative information about carbon impurities in the films<sup>III,VI</sup> and also to characterize the chemical stability of the films.<sup>III</sup> Elemental carbon has been observed in CVD studies of metal beta-diketonates, but in our case the use of a strong oxidizer may have converted it to carbonate. Carbonate species can be identified in IR spectra as bands at 850  $\text{cm}^{-1}$  and a doublet with transmittance maxima at around 1390 and 1470  $\text{cm}^{-1}$  (Fig. 4a). Typically in the  $\text{La}_2\text{O}_3$  films, the carbonate peak area

decreased as the carbon content of films of the same thickness decreased. A similar type of carbonate impurity has been found in ALE-grown  $\text{Y}_2\text{O}_3$  films deposited from yttrium beta-diketonate and ozone precursors.<sup>179</sup>

The IR spectrum presented in Fig. 4b, reveals that the as-deposited cubic  $\text{La}_2\text{O}_3$  films were chemically unstable, absorbing water from the air and slowly transforming to  $\text{LaO}(\text{OH})$  phase during storage. The transformation was seen as a new peak at about  $3450\text{ cm}^{-1}$  caused by hydroxyl group stretching. It was also seen in the XRD patterns of the films where additional peaks of the  $\text{LaO}(\text{OH})$  phase appeared.<sup>III</sup> Further, TOF-ERD analysis indicated film composition corresponding to lanthanum oxide hydroxide,<sup>III</sup> but only after weeks of storage. According to IR spectra, XRD patterns, and TOF-ERD analyses, the films grown at deposition temperatures below  $350\text{ }^\circ\text{C}$  were chemically stable. The origin of peaks observed in Figs. 4c & d is discussed in section 4.1.2.

**Preliminary studies on the growth of NiO and  $\text{Co}_3\text{O}_4$ .**<sup>IV,V</sup> Before the  $\text{LaNiO}_3$  and  $\text{LaCoO}_3$  thin film depositions, preliminary studies were made on the constituent oxides, *viz.* NiO and  $\text{Co}_3\text{O}_4$ . However, only the effect of deposition temperature between  $200$  and  $450\text{ }^\circ\text{C}$  on the film growth was studied. At all temperatures, both NiO and  $\text{Co}_3\text{O}_4$  films had a clear thickness profile in the gas flow direction. A similar profile was recorded in the study of Utriainen *et al.*<sup>181</sup> where NiO films were deposited by ALE from  $\text{Ni}(\text{acac})_2$  and ozone. The authors report that the profile was associated with too low precursor doses and uniform films were obtained only with very long pulses of  $25\text{ s}$  for  $\text{Ni}(\text{acac})_2$  and ozone. Another explanation for the non-uniformity of the films might be that Hthd, formed during the reaction of metal beta-diketonates with the OH groups on the surface, further reacts with the oxide surface and either removes metals as thd complexes or blocks the available reactive surface sites. The etching of the oxide surface with beta-diketonates has been reported in the literature.<sup>182,183</sup> It is also possible that the previously formed oxide layer catalyzes the decomposition of beta-diketonate precursors. Since the cobalt oxide films were non-transparent and dissolving them into mineral acids was not successful, the thickness and growth rate of the cobalt oxide films could not be determined. The NiO films were transparent at all deposition temperatures and a growth rate of about  $0.29\text{ \AA}/\text{cycle}$  was measured at  $350\text{ }^\circ\text{C}$ .

The as-deposited films were crystalline with a cubic NiO or Co<sub>3</sub>O<sub>4</sub> structure between the deposition temperatures 250 and 350 °C. In the case of cobalt oxide, a two-phase mixture of Co<sub>3</sub>O<sub>4</sub> and CoO was observed in the temperature range of 350–400°C. Both cobalt and nickel precursors clearly decomposed at 400 °C, seen, for instance, as a mixture of peaks of NiO and Ni in the XRD patterns.

**Ga<sub>2</sub>O<sub>3</sub>.**<sup>II</sup> Oxygen was not reactive enough to facilitate Ga<sub>2</sub>O<sub>3</sub> thin film growth from Ga(acac)<sub>3</sub> at temperatures between 350 and 400 °C, but temperature-independent, self-limited growth was observed in the Ga(acac)<sub>3</sub>–H<sub>2</sub>O process in the narrow temperature range between 365 and 380 °C. Unfortunately, RBS analysis showed the films to contain a considerable amount of carbon impurity, making this process unsuitable for the processing of high-quality Ga<sub>2</sub>O<sub>3</sub> thin films.

In the Ga(acac)<sub>3</sub>–O<sub>3</sub> process a temperature-independent growth was achieved between 350 and 375 °C. The growth rate was independent of Ga(acac)<sub>3</sub> pulse duration and also the film thicknesses exhibited a linear relation with the number of cycles, confirming that the growth was self-limiting. The growth rate was 0.28 Å/cycle on soda lime glass but a slightly lower 0.21 Å/cycle on silicon. In contrast to the CVD-type growth above 375 °C reported in Publication II, the new experiments carried out in a flow-tube-type reactor with smaller reactor chamber showed that the films were uniform even outside the ALE window, up to 425 °C.<sup>VII</sup> The new series of experiments also gave a somewhat higher growth rate of 0.33 Å per cycle on soda lime glass.

The films deposited with ozone were stoichiometric within the accuracy limits of RBS and only 1 at.% of carbon was detected as an impurity.<sup>II</sup> In addition, TOF-ERD analysis of a 100-nm-thick film grown in the other flow-tube-type reactor at 370 °C showed the film to consist of stoichiometric and pure Ga<sub>2</sub>O<sub>3</sub>, containing less than 0.1 at-% of carbon and hydrogen as impurities. No carbonate group peaks were detected in the IR spectra either. RBS and TOF-ERDA results indicated that the elemental distributions in the films were uniform. The films were amorphous and highly uniform with only 1% thickness variations in the gas flow direction. In addition, the film density of 5.6 g/cm<sup>3</sup> and refractive index of 1.9, which are similar to the values of bulk β-Ga<sub>2</sub>O<sub>3</sub>,<sup>II</sup> verified that the ALE-grown Ga<sub>2</sub>O<sub>3</sub> thin films are of



high quality. In comparison with films prepared by CVD, described in section 2.3.1, the ALE-grown  $\text{Ga}_2\text{O}_3$  films would appear to have lower impurity content and better stoichiometry.

**Preliminary studies on the growth of  $\text{Al}_2\text{O}_3$ .** A new aluminum precursor compatible with the lanthanum precursor,  $\text{La}(\text{thd})_3$ , was required for the  $\text{LaAlO}_3$  film studies.<sup>VI</sup> Since no film growth was detected when  $\text{Al}(\text{thd})_3$  and ozone were used as precursors, studies were focused on  $\text{Al}(\text{acac})_3$  and ozone as the precursors for the growth of  $\text{Al}_2\text{O}_3$  thin film.<sup>VI</sup> A narrow plateau of temperature-independent, self-limited growth with a growth rate of  $0.24 \text{ \AA}/\text{cycle}$  on silicon was observed in the temperature range  $350\text{--}380 \text{ }^\circ\text{C}$ . Above  $380 \text{ }^\circ\text{C}$  and below  $350 \text{ }^\circ\text{C}$  the growth rate increased with temperature. Below  $300 \text{ }^\circ\text{C}$  there was no film formation. The films formed between  $300$  and  $400 \text{ }^\circ\text{C}$  were of uniform thickness both along and across the gas flow direction. TOF-ERD analysis of a film deposited at  $350 \text{ }^\circ\text{C}$  showed it to be stoichiometric  $\text{Al}_2\text{O}_3$ . No peaks of carbonate groups could be detected in the IR spectra.

**Phosphorus-doped  $\text{Al}_2\text{O}_3$ .**<sup>I,184</sup> The ALE growth rate measured for  $\text{Al}_2\text{O}_3$  films deposited at  $500 \text{ }^\circ\text{C}$  using  $\text{AlCl}_3$  and  $\text{H}_2\text{O}$  as precursors was  $0.46 \text{ \AA}/\text{cycle}$ , which is of the same magnitude as found in other ALE studies.<sup>58</sup> The same growth rate was obtained for phosphorus-doped  $\text{Al}_2\text{O}_3$  films when the P/Al atomic ratio in the films was below 1.0. When the P/Al atomic ratio in the films was  $> 1.0$  the growth rate was  $0.35 \text{ \AA}/\text{cycle}$ , indicating that the film growth mechanism changes when more phosphorus is introduced. The growth of phosphorus-doped  $\text{Al}_2\text{O}_3$  films on soda lime glass was similar to the growth on thermally oxidized silicon, since both the P/Al ratio in the films and the film growth rate were the same in films grown simultaneously on different substrates. This result is reasonable, since soda lime glass and  $\text{SiO}_2$ -covered silicon has similar surface sites for reactants to adsorb at.

The film composition was calculated from the elemental concentrations determined by RBS (Table 4). From these data it was concluded that  $\text{Al}_2\text{O}_3$  and  $\text{AlPO}_4$  were simultaneously present. All the films contained chlorine, which is most probably in the form of surface-bound aluminum oxochloride,  $\text{Al}_2\text{Cl}_x\text{O}_{3-x}$ <sup>185,186</sup> and is due to incomplete reaction of aluminum chloride and water. When the P/Al atomic ratio exceeded 1.0, the films were concluded to contain predominantly  $\text{AlPO}_4$ . In addition, since these films had a small surplus of

phosphorus some phosphorus-containing compounds have to exist in the films. The density of the films was close to that of aluminum orthophosphate and their IR spectra resembled those of  $\text{AlPO}_4$ , further indicating that the films were in fact  $\text{AlPO}_4$ . The RBS results showed that the distribution of phosphorus was homogeneous in films where the phosphorus content was greater than 5 at.%. In films with lower phosphorus content the phosphorus was enriched at the film/substrate interface, most probably as a consequence of diffusion. Typically, the films were amorphous, but a weak (210) reflection of aluminum orthophosphate was observed in the XRD patterns of films when the phosphorus concentration exceeded 17 at.%.

**Table 4.** Measured (RBS) concentrations of Al, P and Cl in phosphorus-doped  $\text{Al}_2\text{O}_3$  films and calculated fractions of aluminum orthophosphate and aluminum oxide. The film densities are given. Samples 1-4 were processed with  $\text{P}_2\text{O}_5$  and the rest with TMP as a phosphorus source.

	Total cycles (Al:P ratio)	Al at. %	P at. %	$\text{O}_{\text{meas.}}(\text{O}_{\text{calc.}})$ at. %	$\text{Cl}_{\text{meas.}}(\text{Cl}_{\text{calc.}})$ at. %	$\text{AlPO}_4$ at. %	$\text{Al}_2\text{O}_3$ at. %	Density $\text{g/cm}^3$
1	1430 (5:1)	17.0	19.0	62.5 (64.5)	1.5 (1.5)	96.7	-	2.17
2	700 (10:1)	15.6	17.1	65.5 (65.5)	1.9 (1.9)	93.5	-	2.30
3	220 (30:1)	25.1	10.9	63.1 (63.8)	0.9 (0.9)	64.3	34.8	2.42
4	95 (60:1)	34.1	5.5	59.6 (61.6)	0.9 (0.8)	31.1	68.1	3.12
5	1200 (5:1)	28.8	9.2	61.1 (63.0)	0.9 (0.8)	52.6	46.6	2.70
6	600 (10:1)	31.8	6.0	61.0 (61.6)	1.2 (1.2)	35.6	63.2	2.74
7	230 (30:1)	35.9	2.9	59.9 (60.4)	1.3 (1.2)	17.1	81.7	2.85
8	100 (60:1)	37.7	2.1	59.5 (60.4)	0.7 (0.7)	12.2	87.1	2.92

The chemical behavior of the films was studied by determining etching rates in phosphoric acid at 60 °C. The etching rate of pure aluminum oxide film was 10 nm/min. Films with phosphorus content greater than 5 at.% showed higher etching rates, from 15 nm/min to over 200 nm/min (>17 at.% P). These observations support the conclusion that the films contained both  $\text{Al}_2\text{O}_3$  and  $\text{AlPO}_4$ .

#### 4.1.2 Effect of post-annealing on film crystallinity and properties

$\text{La}_2\text{O}_3$ .<sup>III</sup> The extent and character of crystallization was dependent on the deposition and annealing temperatures, as summarized in Fig 5. A two-phase mixture of cubic and hexagonal

La<sub>2</sub>O<sub>3</sub> was obtained when as-deposited cubic La<sub>2</sub>O<sub>3</sub> was annealed at 800 °C or the amorphous La<sub>2</sub>O<sub>2</sub>CO<sub>3</sub> film was annealed below 900 °C. The as-deposited cubic La<sub>2</sub>O<sub>3</sub> film crystallized as hexagonal La<sub>2</sub>O<sub>3</sub> with a preferred (101) orientation at annealing temperature of 800 °C, whereas only after increase in the annealing temperature to above 900 °C was the hexagonal phase obtained from the amorphous film. According to TOF-ERD analysis, annealing clearly reduced the carbon content of the films.

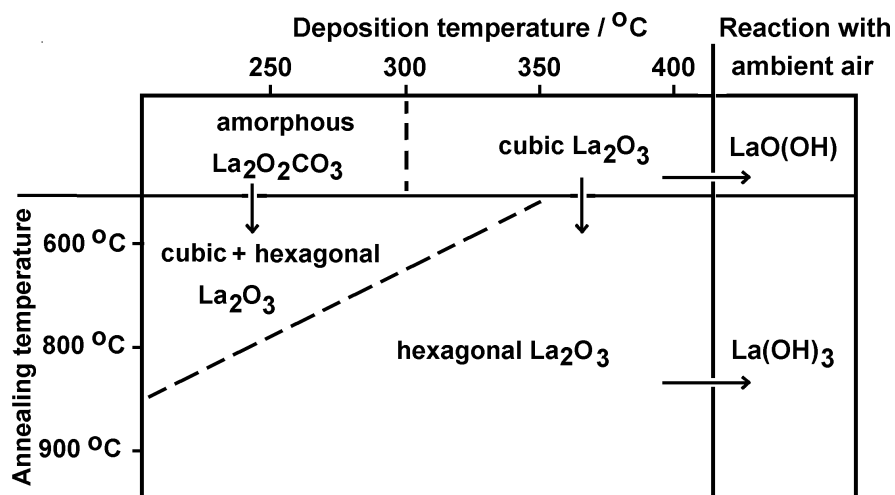


**Figure 5.** Summary of the influence of deposition and annealing temperatures on film composition. Also the effect of ambient air on film quality is shown.<sup>iii</sup>

The IR spectrum, presented in Fig. 4d, revealed that the hexagonal La<sub>2</sub>O<sub>3</sub> films are chemically even more unstable in ambient air than the as-deposited cubic La<sub>2</sub>O<sub>3</sub> films. A relatively quick transformation to lanthanum hydroxide was detected by FTIR, shown as two new peaks at 3610 and 640 cm<sup>-1</sup> due to the OH stretching and La-OH bending modes of the La(OH)<sub>3</sub> phase, respectively. The formation of La(OH)<sub>3</sub> phase was clear in the XRD patterns as well, where after storage of a few days the peaks of hexagonal La<sub>2</sub>O<sub>3</sub> phase completely disappeared and only peaks of hexagonal La(OH)<sub>3</sub> phase were observed.<sup>iii</sup> The chemical instability of the La<sub>2</sub>O<sub>3</sub> films in ambient air is consistent with the results obtained for La<sub>2</sub>O<sub>3</sub> powder material.<sup>187</sup> The rare earth sesquioxides (RE<sub>2</sub>O<sub>3</sub>, RE = element of atomic number 57-71) are known to be basic and they tend to absorb water vapor and carbon dioxide from the atmosphere. The order of basicity decreases with increasing atomic number, lanthanum sesquioxide being the most basic and therefore the most unstable towards reaction with water and acidic carbon dioxide.

## 4.2 Ternary oxides

### 4.2.1 Film growth and composition

**LaNiO<sub>3</sub><sup>IV</sup> and LaCoO<sub>3</sub><sup>V</sup> oxides.** In the first studies on the ALE growth of ternary oxides, the approach was to grow one monolayer of each binary oxide alternately over the top of the other. On the basis of the growth rates of the constituent binary oxides, the following pulsing sequence was chosen:  $N \times [15 \times (\text{La}(\text{thd})_3 + \text{O}_3) + 15 \times (M(\text{thd})_2 + \text{O}_3)]$ , where  $N$  is the number of deposition cycles (“basic cycles”) and  $M$  is Ni or Co. The number of basic cycles ( $N$ ) was varied to obtain films of different thickness.

Only the effects of deposition temperature and number of deposition cycles on the film growth were studied. On the basis of the studies on binary metal oxides, most of the growth experiments were done in the temperature range 200–400 °C. As shown in Fig. 6, the growth rates of both LaNiO<sub>3</sub> and LaCoO<sub>3</sub> films increased as the deposition temperature increased. In the case of LaNiO<sub>3</sub>, the growth rate seemed to be constant in the temperature region from 215 to 250 °C, indicating a possible ALE window. However, as the thickness determination of these rather thin films (<70 nm) was not very accurate, the existence of an ALE window is not certain. Because the growth rates for LaNiO<sub>3</sub> and LaCoO<sub>3</sub> were very low below deposition temperature of 300 °C, further deposition studies were made at higher temperatures.

The film growth was sufficiently reproducible at higher temperatures. The thickness of both LaNiO<sub>3</sub> and LaCoO<sub>3</sub> films could be controlled by the number of deposition cycles (see Fig. 6, inset). The growth rate of LaNiO<sub>3</sub> at 400 °C was 0.25 Å/cycle while that of LaCoO<sub>3</sub> at 350 °C was 0.35 Å/cycle. All the LaNiO<sub>3</sub> and LaCoO<sub>3</sub> films deposited between 200–400 °C exhibited similar thickness profiles in the gas flow direction to those observed in the binary metal oxide depositions of NiO and Co<sub>3</sub>O<sub>4</sub> (discussed in section 4.1.1). This type of thickness profile is also seen in LaMnO<sub>3</sub> and MnO<sub>x</sub> films.<sup>188</sup> Since the La<sub>2</sub>O<sub>3</sub> films deposited in the same reactor were highly uniform, it is unlikely that the profile is related to reactor gas flow characteristics. More likely it is explained by the etching effect of the released Hthd. This type of etching was detected by Haukka *et al.*,<sup>182</sup> in a study where mixed oxides of LaCeCuO and MgMnCoO were deposited on high surface area alumina. Of the single oxide layers they processed, cobalt and copper oxide were the most heavily etched. Haukka *et al.*<sup>182</sup> concluded that for example, cobalt, easily changes its oxidation state and can be etched both as Co(thd)<sub>2</sub> and as Co(thd)<sub>3</sub>.

Furthermore, both cobalt and nickel oxides are known to be catalytically active materials and therefore may catalyze the decomposition of beta-diketonate precursors leading to non-uniform film thicknesses.

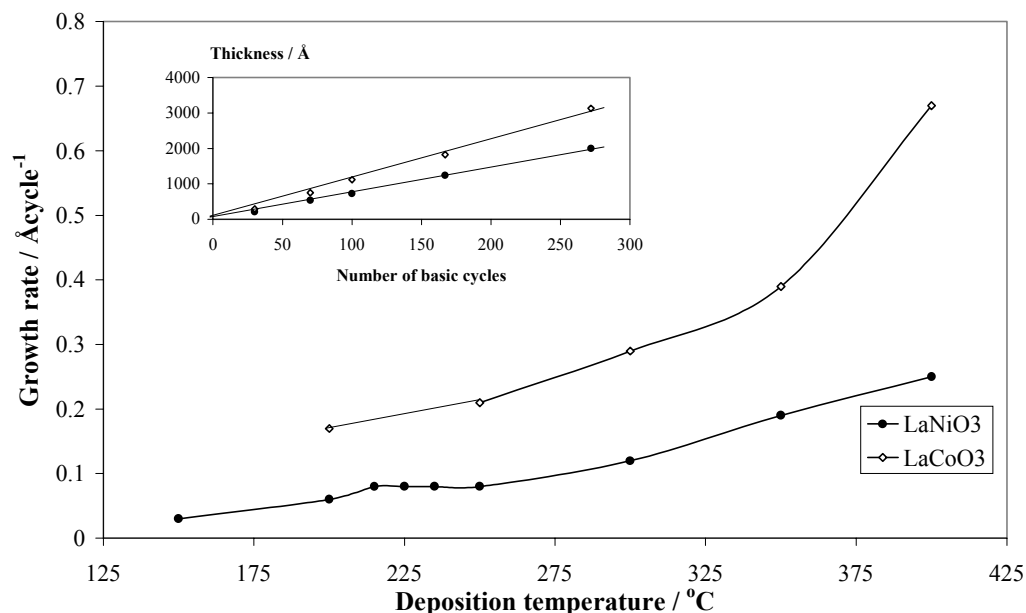


**Figure 6.** Dependence of LaNiO<sub>3</sub> and LaCoO<sub>3</sub> film growth rates on the deposition temperature. The inset shows the dependence of LaNiO<sub>3</sub> and LaCoO<sub>3</sub> film thickness on the number of basic cycles ( $N$ ) at deposition temperatures of 400 °C and 350 °C, respectively.

XPS analysis indicated that the as-deposited LaNiO<sub>3</sub> films consisted of separate oxide layers that reacted only during annealing. According to the RBS and XPS data, no discrete layers were present in the as-deposited LaCoO<sub>3</sub> films. However, the La/Co content ratio in the film deposited at 350 was nearly 1.5, indicating that the film contained a phase mixture of LaCoO<sub>3</sub> and Co<sub>3</sub>O<sub>4</sub>. The carbon content in LaCoO<sub>3</sub> films determined by RBS was 2-3 at.% on the surface but below 0.5 at.% in the bulk.

**LaAlO<sub>3</sub><sup>VI</sup> and LaGaO<sub>3</sub><sup>VII</sup> oxides.** Since the studies on LaNiO<sub>3</sub> and LaCoO<sub>3</sub> film growth showed these films to contain either separate oxide layers or an excess of one metal oxide, a new approach was adopted for studies on LaAlO<sub>3</sub> and LaGaO<sub>3</sub> films. The following pulsing sequence was selected:  $N \times [A \times (\text{La}(\text{thd})_3 + \text{O}_3) + B \times (M(\text{thd})_3 + \text{O}_3)]$ , where  $N$  is the number of deposition cycles,  $A$  and  $B$  have a value between 1 and 7 and  $M$  is Al or Ga. The objective

here was to mix (La-O) and (M-O) deposition cycles as completely as possible and to control the La/M ratio in the films by changing the precursor pulsing ratio ( $A/B$ ). The results for the respective binary oxides suggested study of the film growth in the temperature range 325–425 °C. Films of different thickness were grown by varying the number of deposition cycles.

For both films, the film composition was linearly related to the precursor pulsing ratio at all temperatures studied (see Fig. 7). This means that stoichiometric films can be grown at any deposition temperature between 325 and 425 °C by selecting a suitable precursor pulsing ratio. Stoichiometric  $\text{LaAlO}_3$  films were obtained at temperatures between 350 and 375 °C with the La/Al precursor pulsing ratio of 1.75-2.0, while stoichiometric  $\text{LaGaO}_3$  films were obtained in the temperature region 350–390 °C with the La/Ga precursor pulsing ratio of 2.5. All films, whatever the La/M ( $M=\text{Al,Ga}$ ) atomic ratio, were of uniform thickness both along and across the gas flow direction. The thickness of the films was in linear relation with the number of deposition cycles, and growth rates on silicon substrate were 0.39 Å/cycle for  $\text{LaAlO}_3$  at 375 °C and 0.40 Å/cycle for  $\text{LaGaO}_3$  at 370 °C. The composition of films of different thickness was the same, showing that the growth was well controlled.

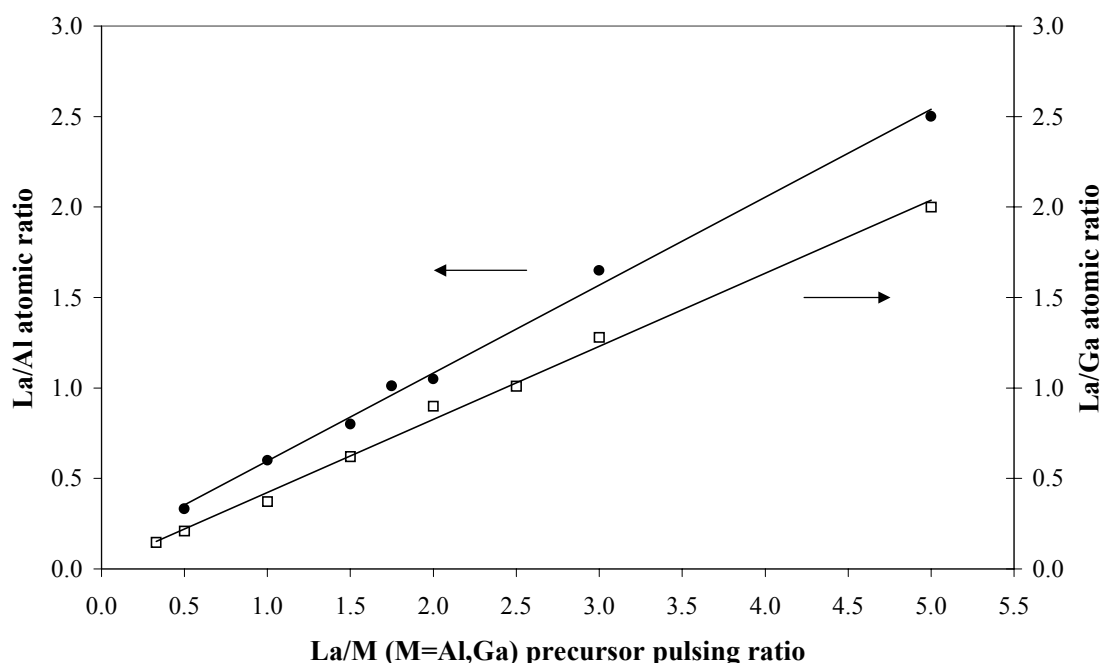


**Figure 7.** La/Al atomic ratio in  $\text{LaAlO}_3$  films deposited at 350 °C and La/Ga atomic ratio in  $\text{LaGaO}_3$  films deposited at 370 °C as a function of the precursor pulsing ratio. Both films were deposited on silicon(100) substrates.

The film growth rates were the same at different  $La/M$  ( $M=Al,Ga$ ) pulsing ratios and, expressed relative to the theoretical growth rates calculated from the measured growth rates of the separate oxides, they clearly decreased as the number of La-O cycles increased.<sup>VI,VII</sup> It seems that the growth of the La-O layer was inhibited by the already formed Al-O or Ga-O surface. Possibly either the surface sites available were not favorable for the adsorption of  $La(thd)_3$  or the bonding mode of  $La(thd)_3$  on the Al-O or Ga-O surface differed from that on the La-O surface.

The stoichiometric  $LaAlO_3$  and  $LaGaO_3$  contained small amounts of the common impurities, carbon and hydrogen. Fluorine contamination was detected as well, possibly originating from the reactor. Less than 1.9 at.% carbon and about 0.3 at.% hydrogen were detected in  $LaAlO_3$  films, and still less impurities were found in  $LaGaO_3$  films, namely 0.4 at.% carbon and less than 0.2 at.% hydrogen. In both films the carbon was mainly related to the La-O part of the film as it was observed that typically the carbon content of the films decreased as the  $La/M$  atomic ratio in the films decreased. The FTIR spectra suggested that carbon is mainly present as carbonate-type impurity. The depth distributions of lanthanum, aluminum and gallium in the films deposited on silicon were uniform as shown in Fig. 8. Also the interfaces of  $LaAlO_3/Si$  and  $LaGaO_3/Si$  were well defined and no diffusion was detected.

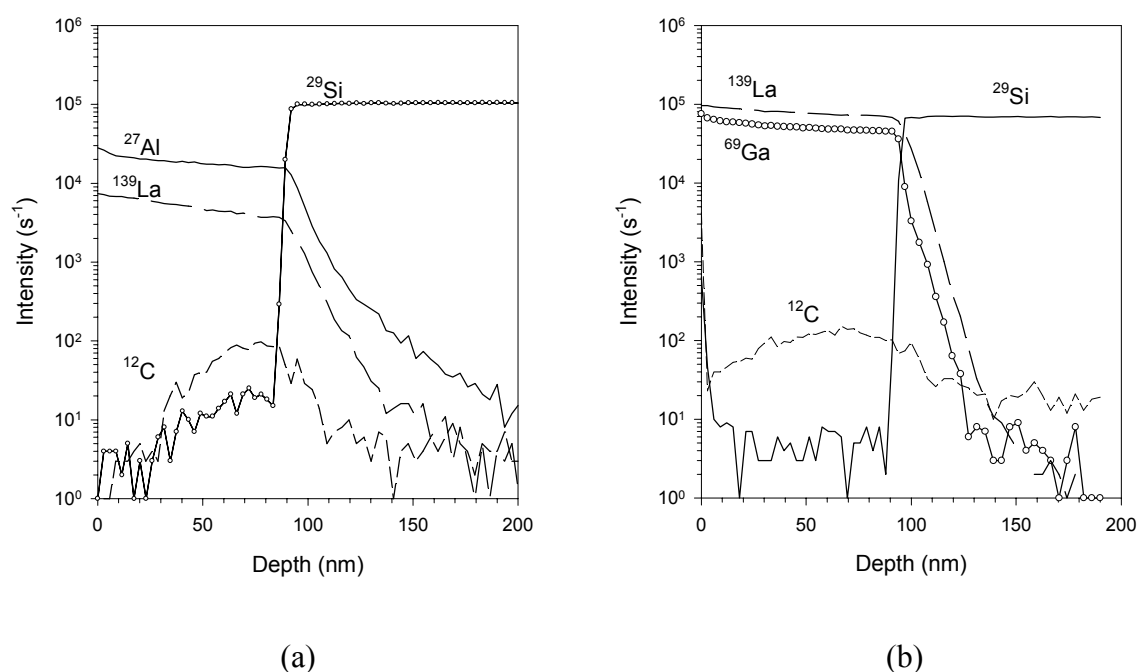


**Figure 8.** SIMS depth profiles of the as-deposited 100-nm-thick  $LaAlO_3$  (a) and  $LaGaO_3$  (b) films deposited on silicon(100) substrates.

## 4.2.2 Crystallinity and morphology

The effect of deposition temperature on the crystallinity of the films is presented in Table 5. Consistent with results reported in the literature (see section 2.3.2), the low deposition temperature resulted in amorphous films. The materials used for construction of the ALE reactor restrict the available deposition temperatures to 500 °C and below, which in the case of LaAlO<sub>3</sub> and LaGaO<sub>3</sub> is too low to obtain crystalline films. In the case of LaNiO<sub>3</sub> and LaCoO<sub>3</sub> films, crystalline films were obtained at temperatures above 400 °C, but they were of poor quality and the XRD patterns indicated phase mixtures of La<sub>2</sub>NiO<sub>4</sub>/NiO or LaCoO<sub>3</sub>/La<sub>4</sub>Co<sub>3</sub>O<sub>10</sub>/Co<sub>3</sub>O<sub>4</sub>, showing that the perovskite was either fully or partially decomposed. As regards stability, many LaMO<sub>3</sub> (*M*=transition metal) perovskites are highly sensitive to changes in temperature and oxygen partial pressure.<sup>6</sup> The reduction of transition metals at high temperatures and/or under low oxygen partial pressure leads to decomposition of the perovskite. In the present study, nitrogen gas was used as purge gas to separate the precursor pulses, and the thin films remained in nitrogen atmosphere during cooling. Probably this caused the decomposition of the films at higher deposition temperatures. Deposition of crystalline LaNiO<sub>3</sub> and LaCoO<sub>3</sub> films might be successful at deposition temperatures above 450 and 400 °C, respectively, but this probably would require the use of oxygen as a carrier gas or cooling in oxygen atmosphere, or both. Furthermore, thermal decomposition of the precursors above 400 °C argues for the use of more stable precursors.

**Table 5.** Crystallinity and phase purity of the LaMO<sub>3</sub> films (*M*=Ni, Co, Al or Ga) at different deposition temperatures, as studied by XRD.

Film material	Deposition temperature			
	≤ 350 °C	400-425 °C	450 °C	500 °C
LaNiO <sub>3</sub>	Amorphous	Amorphous	LaNiO <sub>3</sub>	La <sub>2</sub> NiO <sub>4</sub> /NiO
LaCoO <sub>3</sub>	Amorphous	LaCoO <sub>3</sub> /La <sub>4</sub> Co <sub>3</sub> O <sub>10</sub> /Co <sub>3</sub> O <sub>4</sub>	— <sup>a</sup>	— <sup>a</sup>
LaAlO <sub>3</sub>	Amorphous	Amorphous	— <sup>a</sup>	— <sup>a</sup>
LaGaO <sub>3</sub>	Amorphous	Amorphous	— <sup>a</sup>	— <sup>a</sup>

<sup>a</sup>Not studied.

AFM measurements showed that the as-deposited amorphous films consisted of small crystallites and the roughness of the films was the same or even less than the roughness of the substrate, typical of ALE-type of growth of amorphous films.



### 4.2.3 Effect of post-annealing on film crystallinity and properties

*Ex situ* post-annealing was required to obtain crystalline films. The annealing studies were made in a tube furnace under air or oxygen atmosphere as well as in a rapid thermal annealing furnace under nitrogen atmosphere.

**LaNiO<sub>3</sub><sup>IV</sup> and LaCoO<sub>3</sub><sup>V</sup> oxides.** Crystalline films were obtained when the as-deposited films were annealed at 600 °C in air or oxygen atmosphere. The XRD patterns of annealed LaNiO<sub>3</sub> and LaCoO<sub>3</sub> films showed no splitting of reflections due to rhombohedral distortion, indicating that both films crystallized with polycrystalline cubic structure. This is consistent with the earlier reports on LaNiO<sub>3</sub> and LaCoO<sub>3</sub> thin films deposited by other techniques, reviewed in section 2.3.2. Since amorphous Corning glass was used as substrate, epitaxial or strongly textured growth was not to be expected. Furthermore, an excess of Co<sub>3</sub>O<sub>4</sub> was detected by RBS and XRD in the LaCoO<sub>3</sub> films deposited at 350 °C and 400 °C after annealing. SEM images of LaNiO<sub>3</sub> indicated that the annealed films had non-porous and smooth surfaces without cracks. Some films contained small amounts of spherical particles or droplets on the surface, as was seen also in LaNiO<sub>3</sub> films deposited by other methods.<sup>124</sup> As regards the electrical resistivity of LaNiO<sub>3</sub> films, this varied from 320 Ω cm for the amorphous as-deposited film to 540 μΩ cm for the same film after annealing and crystallization. The latter value is of the same order of magnitude as found for polycrystalline LaNiO<sub>3</sub> films deposited by other thin film deposition methods, as reviewed in section 2.3.2.

**LaAlO<sub>3</sub><sup>VI</sup> and LaGaO<sub>3</sub><sup>VII</sup> oxides.** Obtaining crystalline films required post-annealing temperatures of 900 °C for LaAlO<sub>3</sub> and 850 °C for LaGaO<sub>3</sub>. Both films crystallized as perovskite phase having a pseudocubic structure. As shown in Table 6, the substrate employed had a marked influence on the crystallinity of the films. Epitaxial LaAlO<sub>3</sub> and LaGaO<sub>3</sub> films, presented in Fig. 9, were obtained only on perovskite-type single-crystal substrates, *e.g.* SrTiO<sub>3</sub> and LaAlO<sub>3</sub>. These films had a very smooth surface with a surface roughness of 1.1 nm. Compared with the best results for LaAlO<sub>3</sub> films deposited on perovskite-type single-crystal substrates by other CVD methods,<sup>156,157</sup> the ALE-grown films appear to have better crystalline quality and smoother surfaces. The benefit of the ALE process seems to be that the amorphous film obtained has a suitable stoichiometry and perfect surface morphology for

efficient re-crystallization in the thermal annealing process. The films deposited on sapphire and single-crystal MgO(100) were polycrystalline with the (110) reflection being the most intense. These results are consistent with the results of other groups reviewed in section 2.3.2, where epitaxial growth was achieved on lattice-matched substrates, while randomly or slightly oriented films were obtained on non-lattice matched substrates.

**Table 6.** Crystal quality of annealed LaAlO<sub>3</sub> and LaGaO<sub>3</sub> films deposited onto various substrates.

Substrate	LaAlO <sub>3</sub> thin films		LaGaO <sub>3</sub> thin films
	Annealed at 900 °C	Annealed at 950 °C	Annealed at 850 °C
SrTiO <sub>3</sub> (100)	Epitaxial LaAlO <sub>3</sub>	Epitaxial LaAlO <sub>3</sub>	Epitaxial LaGaO <sub>3</sub>
LaAlO <sub>3</sub> (100)	— <sup>a</sup>	— <sup>a</sup>	Epitaxial LaGaO <sub>3</sub>
Sapphire	Polycrystalline LaAlO <sub>3</sub> , (110) most intense	Polycrystalline LaAlO <sub>3</sub> , (110) most intense	Polycrystalline LaGaO <sub>3</sub> , (110) most intense
MgO(100)	— <sup>a</sup>	— <sup>a</sup>	Polycrystalline LaGaO <sub>3</sub> , (110) most intense
Si(100)	Polycrystalline LaAlO <sub>3</sub> , (110) oriented	Highly crystalline La <sub>4</sub> Al <sub>2</sub> O <sub>9</sub> + LaAlO <sub>3</sub>	Highly crystalline La <sub>4</sub> Ga <sub>2</sub> O <sub>9</sub> + LaGaO <sub>3</sub>
MgO(100)-buffered Si(100)	Polycrystalline LaAlO <sub>3</sub> , slightly (100) oriented	LaAlO <sub>3</sub> + La <sub>4</sub> Al <sub>2</sub> O <sub>9</sub>	Highly crystalline La <sub>4</sub> Ga <sub>2</sub> O <sub>9</sub> + LaGaO <sub>3</sub>
MgO(111)-buffered Si(100)	Polycrystalline LaAlO <sub>3</sub> , (110) oriented	LaAlO <sub>3</sub> + La <sub>4</sub> Al <sub>2</sub> O <sub>9</sub>	Highly crystalline La <sub>4</sub> Ga <sub>2</sub> O <sub>9</sub> + LaGaO <sub>3</sub>

<sup>a</sup>Not deposited.

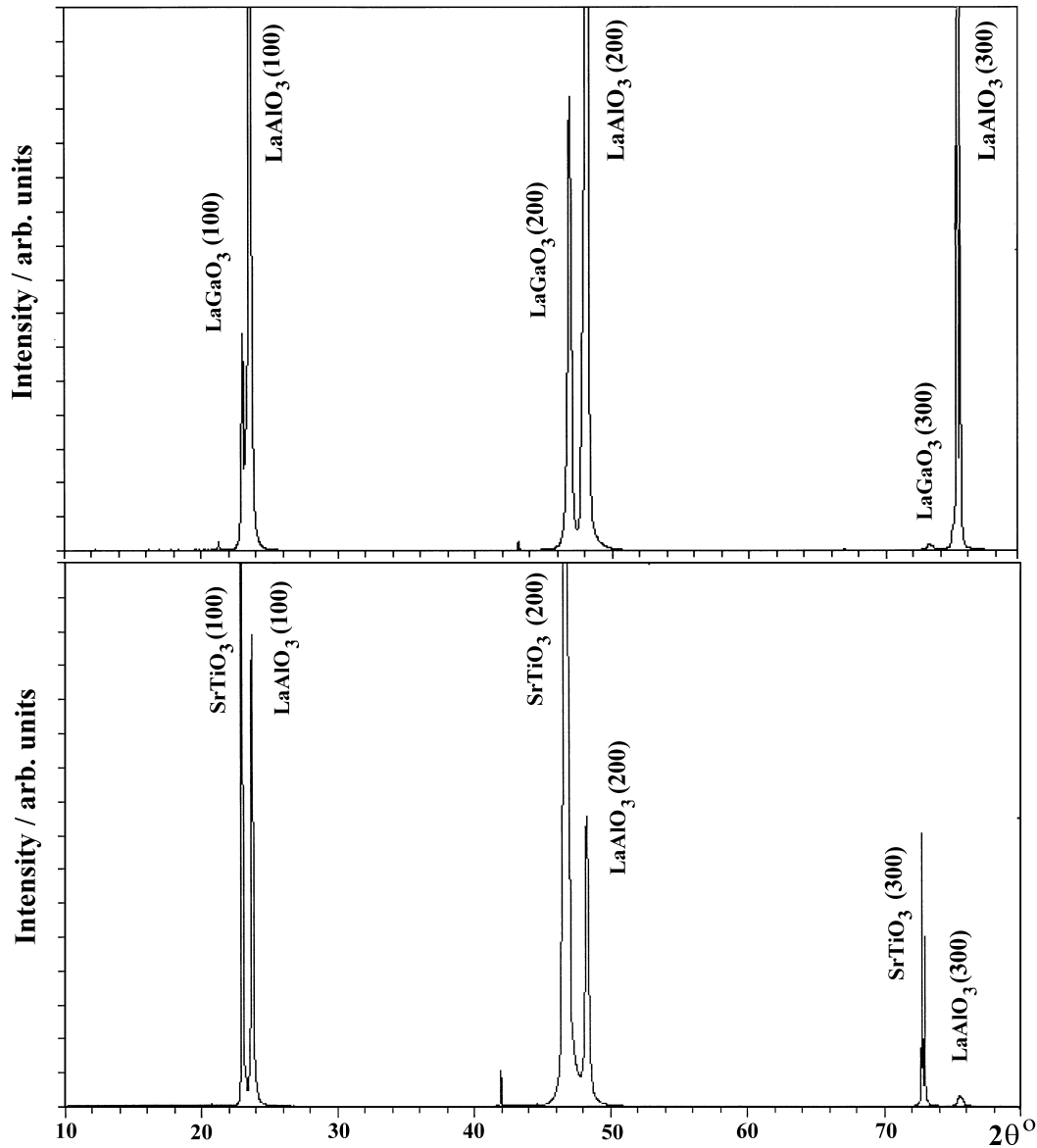


**Figure 9.** XRD patterns of epitaxial LaGaO<sub>3</sub> film deposited on LaAlO<sub>3</sub>(100) substrate and LaAlO<sub>3</sub> film deposited on SrTiO<sub>3</sub>(100) substrate after post-annealing in N<sub>2</sub> at 900 and 850 °C for 30 min, respectively.

LaAlO<sub>3</sub> films with (110) orientation were obtained on Si(100) at 900 °C, but interdiffusion between film and substrate was observed when the annealing temperature was raised to 950 °C. In the case of LaGaO<sub>3</sub>, the interdiffusion occurred at 850 °C and a crystalline LaGaO<sub>3</sub> phase was not observed on silicon. In both cases, where silicon diffused into the film highly crystalline La<sub>4</sub>M<sub>2</sub>O<sub>9</sub> ( $M=Al,Ga$ ) phase was detected in XRD patterns as the main phase and small peaks of LaMO<sub>3</sub> ( $M=Al,Ga$ ) were observed as a secondary phase (Table 5). As

demonstrated by the SIMS depth profiles in Fig. 10, the diffusion was more pronounced in the LaGaO<sub>3</sub> films.

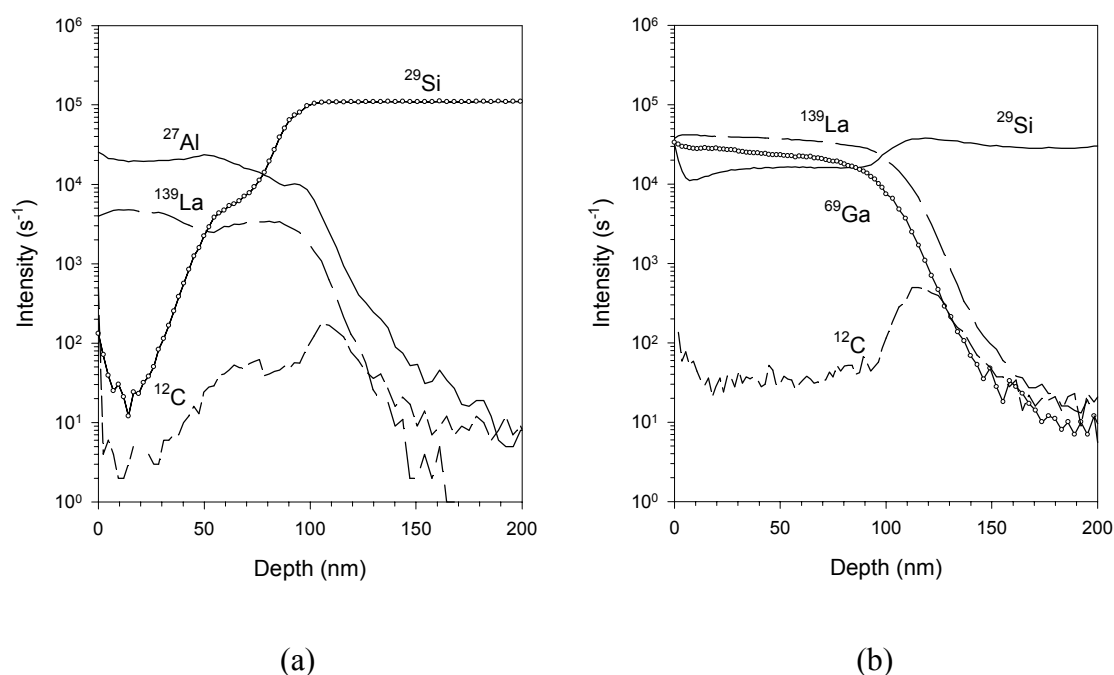


**Figure 10.** SIMS depth profiles of the 100-nm-thick LaAlO<sub>3</sub> (a) and LaGaO<sub>3</sub> (b) thin films deposited on silicon(100) substrates and annealed at 950 and 850 °C in N<sub>2</sub> for 30 min, respectively.

The surface roughness of films deposited on silicon and annealed at different temperatures was typically below 1.0 nm, indicating very smooth surfaces. The columnar-type growth seen in the AFM images of the annealed La-Al-O films was not observed in those of the La-Ga-O films. Deep cracks appeared on the surface of the La-Al-O films annealed at 950 °C, but no cracks were observed in the La-Ga-O films annealed at 850 °C.

To study whether the mixing of the silicon substrate and LaAlO<sub>3</sub> or LaGaO<sub>3</sub> film during annealing could be prevented, films were also deposited on MgO-buffered Si(100) substrates. The ALE-grown MgO-buffer layers had either a preferred (100) or (111) orientation.<sup>189,190</sup> Thin LaAlO<sub>3</sub> films (<100 nm) grown on (100) or (111) oriented MgO and annealed at 900 °C had (100) or (110) preferred orientations, respectively, but when the annealing temperature was raised to 950 °C an additional La<sub>4</sub>Al<sub>2</sub>O<sub>9</sub> phase was observed in the XRD patterns. However, if the thickness of MgO-buffer layer or LaAlO<sub>3</sub> film exceeded 100 nm, the films mostly contained the LaAlO<sub>3</sub> phase. In the case of LaGaO<sub>3</sub>, all films deposited on MgO-

buffered silicon and annealed at 850 °C predominantly crystallized as the  $\text{La}_4\text{Ga}_2\text{O}_9$  phase, irrespective of the thickness of buffer layer or film.

The SIMS depth profiles (Figs. 11a and 5c in publication VII) indicated that the interfaces of  $\text{LaGaO}_3/\text{MgO}$  and  $\text{LaAlO}_3/\text{MgO}$  were well defined in the as-deposited films and no diffusion was detected. In the annealed films, containing the  $\text{La}_4M_2\text{O}_9$  ( $M=\text{Al,Ga}$ ) phase,  $\text{MgO}$ -buffer layer prevented the diffusion of silicon, but instead magnesium diffused through the films (Figs. 11b and 5d in publication VII). The diffusion of magnesium was somewhat surprising, because  $\text{MgO}$  was expected to be stable and it had been successfully used as a substrate by another group.<sup>156</sup> The obtaining of polycrystalline  $\text{LaGaO}_3$  films on single-crystal  $\text{MgO}$  substrate (see Table 5) suggests that the  $\text{MgO}$  films grown by ALE are not stable at high annealing temperatures. Probably this is because of their polycrystalline structure.

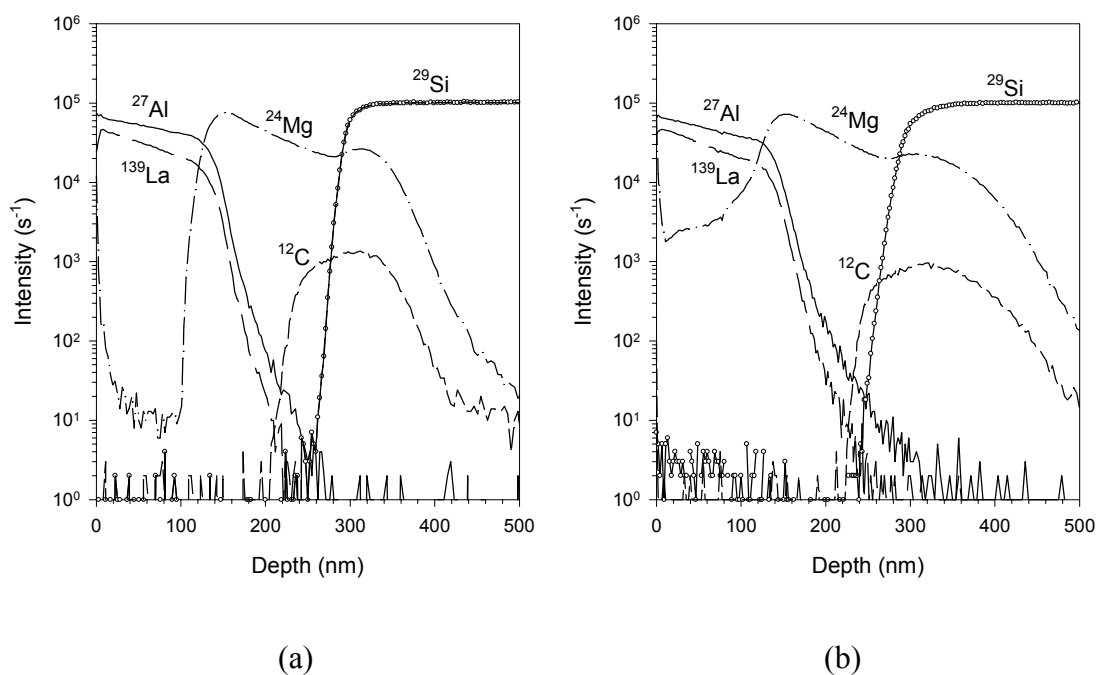


**Figure 11.** SIMS depth profiles of the 100-nm-thick  $\text{LaAlO}_3$  films deposited on  $\text{MgO}$ -buffered silicon: as-deposited amorphous film (a) and the same film after annealing at 950 °C in  $\text{N}_2$  for 30 min (b).

The SIMS depth profiles also showed gallium to diffuse towards the La-Ga-O/MgO interface and even through the MgO layer into the silicon substrate (Fig. 5d in publication VII); no corresponding phenomenon was detected in the case of LaAlO<sub>3</sub> (Fig. 11b). The La/*M* (*M*=Al,Ga) atomic ratio in the bulk of the annealed films deposited on silicon or MgO-buffered silicon as determined by RBS differed from the La/*M* ratio of the La<sub>4</sub>*M*<sub>2</sub>O<sub>9</sub> phase determined by XRD. Probably part of the aluminum and gallium is in the form of amorphous oxide on grain boundaries and therefore not detected by XRD.

It can be concluded that the diffusion of silicon or magnesium into LaAlO<sub>3</sub> or LaGaO<sub>3</sub> films initiates the formation of the La<sub>4</sub>*M*<sub>2</sub>O<sub>9</sub> (*M*=Al,Ga) phase. However, it is not clear why silicon and magnesium diffuse more easily (at a lower temperature) into the LaGaO<sub>3</sub> film than into the LaAlO<sub>3</sub> film.

## CONCLUSIONS

Metal oxides have a wide range of chemical, electrical, optical, and magnetic properties that make them of interest for applications in thin film technology. Among the many techniques used for depositing thin films, atomic layer epitaxy (ALE) uniquely offers controlled growth of high quality films onto large area substrates. So far, the majority of ALE thin film studies have focused on binary systems of metal oxides, nitrides, and sulfides and the growth of binary oxides by ALE is fairly straightforward. The growth of ternary oxides remains a challenge, because achieving the correct stoichiometry is much more difficult. In the present thesis, the preparation of the ternary oxide thin films  $\text{LaNiO}_3$ ,  $\text{LaCoO}_3$ ,  $\text{LaAlO}_3$ , and  $\text{LaGaO}_3$  by ALE technique has been studied. First, preliminary studies were carried out on the ALE growth of the binary metal oxides  $\text{NiO}$ ,  $\text{Co}_3\text{O}_4$ , and  $\text{Al}_2\text{O}_3$  and more detailed studies on the growth of  $\text{La}_2\text{O}_3$ , and  $\text{Ga}_2\text{O}_3$  films. In addition, modification of the  $\text{Al}_2\text{O}_3$  films by phosphorus doping was studied.

The binary and ternary oxides were deposited from metal beta-diketonates and ozone precursors. In the case of the  $\text{Al}_2\text{O}_3$  and  $\text{Ga}_2\text{O}_3$  films, the growth was temperature-independent and self-limiting and films were stoichiometric, pure, dense, and uniform. Thus, both processes were considered applicable for the ternary oxide growth studies. The  $\text{La}_2\text{O}_3$  phase was formed only at higher temperatures, where the growth rate increased with temperature. In addition, the  $\text{La}_2\text{O}_3$  films contained a small amount of carbon impurity. However, since growth was well controlled and films were uniform at these higher temperatures, the  $\text{La}_2\text{O}_3$  process, too, was considered applicable for the ternary oxide growth studies. The  $\text{NiO}$  and  $\text{Co}_3\text{O}_4$  films, in contrast, showed variations in thickness at all temperatures studied. Evidently the changes in oxidation state of the transition metal makes the thin film growth of these metal oxides very complicated, a problem that could not be solved in this work. The growth rates of all films deposited from metal beta-diketonates and ozone were much less than one monolayer per cycle, probably because of steric hindrance due to the bulky metal beta-diketonate molecules. Both  $\text{Al}_2\text{O}_3$  and  $\text{Ga}_2\text{O}_3$  films were amorphous, whereas the  $\text{NiO}$ ,  $\text{Co}_3\text{O}_4$  and  $\text{La}_2\text{O}_3$  films were polycrystalline with a cubic structure. The phosphorus-doped  $\text{Al}_2\text{O}_3$  films deposited from  $\text{AlCl}_3$ ,  $\text{P}_2\text{O}_5$  or trimethyl-phosphate, and water were amorphous as well. At heavy phosphorus doping the  $\text{AlPO}_4$  phase was formed as predominant phase; otherwise the films consisted of both  $\text{Al}_2\text{O}_3$  and  $\text{AlPO}_4$ .

The ALE process used for growing the  $\text{LaNiO}_3$  and  $\text{LaCoO}_3$  films was not optimal. The approach chosen was to grow monolayers of the constituent binary oxides alternately on top of one another. In the case of  $\text{LaNiO}_3$ , this resulted in films consisting of separate layers of the lanthanum and nickel oxides, which reacted only during annealing to form  $\text{LaNiO}_3$ . In the case of  $\text{LaCoO}_3$ , excess of cobalt resulted. A better approach is to sequentially grow submonolayers of the two constituent oxides so that the oxide structure is better mixed. A stoichiometric ratio of the two metals in the films is achieved by applying the appropriate precursor pulsing ratio. With this improved approach, stoichiometric and pure  $\text{LaAlO}_3$  and  $\text{LaGaO}_3$  films with a uniform depth distribution of metals were deposited.

All the as-deposited ternary oxide films were amorphous but crystallized with cubic structure when post-annealed. Even though good quality films were obtained after annealing, growth of crystalline films inside the ALE reactor would be preferred. The materials currently used for construction of the ALE reactor set an upper limit for the deposition temperature at around  $500\text{ }^\circ\text{C}$ , which is too low to obtain crystalline  $\text{LaAlO}_3$  and  $\text{LaGaO}_3$ . In the case of  $\text{LaNiO}_3$  and  $\text{LaCoO}_3$ , it might be possible to obtain crystalline films between deposition temperatures  $400$  and  $500\text{ }^\circ\text{C}$ , but more stable precursors would then be needed. In addition, the decomposition of the transition metal perovskite due to the reduction of the transition metal at high temperatures and low oxygen partial pressure is a problem that needs addressing.

To conclude, the present work has shown that after optimization of the processing parameters, some of the general advantages of the ALE method, such as excellent control of stoichiometry, thickness, and uniformity of the films, can be achieved for both the binary metal oxides and the perovskite-type oxides. Even though ALE has already been proven itself a versatile method for the controlled processing of binary oxide films, the capability of ALE for producing the more complex ternary oxide thin films opens up new prospects for the ALE technique.



## REFERENCES

1. Suntola, T. and Antson, J., *Finnish Patent No. 52 359* (1974).
2. Suntola, T. and Antson, J., *U. S. Patent No. 4 058430* (1977).
3. Suntola, T., *Mater. Sci. Rep.* **4** (1989) 261.
4. Suntola, T., in *Handbook of Crystal Growth*, Vol **3**, Hurle, D.T.J., (Ed.), Elsevier, Amsterdam 1994, 601.
5. Ritala, M. and Leskelä, M., in *Handbook of Thin Film Materials*, Vol **1**, Nalwa, H.S., (Ed.), Academic Press, San Diego 2001, 103.
6. Seim H., *Doctoral thesis*, University of Oslo, Oslo 1997, 80p.
7. Niinistö, L., *Proc. Int. Semicond. Conf. CAS* **1** (2000) 33.
8. Niinistö, L., *Current Opinion in Solid State & Materials Science* **3** (1998) 147.
9. Leskelä, M. and Ritala, M., *Thin Solid Films*, in press.
10. Ritala, M. and Leskelä, M., *Nanotechnology* **10** (1999) 19.
11. Suntola, T., Antson, J., Pakkala, A., and Lindfors, S., *SID 80 Digest* (1980) 108.
12. Niinistö, L., Ritala, M., and Leskelä, M., *Mater. Sci. Eng. B* **41** (1996) 23.
13. Jeong, C-W., Lee, J-S., and Joo, S-K., *Jpn. J. Appl. Phys.* **40** (2001) 285.
14. Putkonen, M., Nieminen, M., Niinistö, J., and Niinistö, L., *Chem. Mater.*, in press.
15. Kosola, A., Päiväsaari, J., and Niinistö, L., to be published.
16. Päiväsaari, J. and Niinistö, L., to be published.
17. Rahtu, A., Kukli, K., and Ritala, M., *Chem. Mater.* **13** (2001) 817.
18. Aarik, J., Aidla, A., Mändar, H., and Sammelselg, V., *J. Cryst. Growth* **220** (2000) 531.
19. Aarik, J., Aidla, A., Uustare, T., Ritala, M., and Leskelä, M. *Appl. Surf. Sci.* **161** (2000) 385.
20. Schuisky, M., Hårsta, A., Aidla, A., Kukli, K., Kiisler, A-A., and Aarik, J., *J. Electrochem. Soc.* **147** (2000) 3319.
21. Kukli, K., Aidla, A., Aarik, J., Schuisky, M., Hårsta, A., Ritala, M., and Leskelä, M. *Langmuir* **16** (2000) 8122.
22. Kukli, K., Ritala, M., Schuisky, M., Leskelä, M., Keinonen, M., Uustare, T., and Hårsta A., *Chem. Vap. Deposition* **6** (2000) 303.
23. Putkonen, M. and Niinistö, L., *J. Mater. Chem.*, in press.
24. Perkins, C.M., Triplett, B.B, McIntyre, P.C., Saraswat, K.C., Haukka, S., and Tuominen, M., *Appl. Phys. Lett.* **78** (2001) 2357.

25. Kukli, K., Ritala, M., and Leskelä, M., *Chem. Vap. Deposition* **6** (2000) 297.
26. Aarik, J., Aidla, A., Mändar, H., Sammelselg, V., and Uustare, T., *J. Cryst. Growth* **220** (2000) 105.
27. Badot, J.C., Ribes, S., Yousfi, E.B., Vivier, V., Pereira-Ramos, J.P., Baffier, N., and Lincot, D., *Electrochem. Solid State Lett.* **3** (2000) 485.
28. Kukli, K., Aarik, J., Aidla, A., Forsgren K., Sundqvist, J., Hårsta, A., Uustare, T., Mändar, H., and Kiisler, A-A., *Chem. Mater.* **13** (2001) 122.
29. Kukli, K., Ritala, M., and Leskelä M., *Chem. Mater.* **12** (2000) 1914.
30. Kaiya, K., Yoshii, N., Omichi, K., Takahashi, N., Nakamua, T., Okamoto, S., and Yamamoto, H., *Chem. Mater.* **13** (2001) 1952.
31. Yousfi, E.B., Weinberger, B., Donsanti, F., Cowache, P., and Lincot, D., *Thin Solid Films* **387** (2001) 29.
32. Vehkamäki, M., Hänninen, T., Ritala, M., Leskelä, M., Sajavaara, T., Rauhala, E., and Keinonen, J., *Chem. Vap. Deposition* **7** (2001) 75.
33. Rahtu, A., Ritala, M., and Leskelä, M., *Chem. Mater.* **13** (2001) 1528.
34. Zhang, H. and Solanki, R. *J. Electrochem. Soc.* **148** (2001) F63.
35. Kukli, K., Ritala, M., and Leskelä, M., *J. Electrochem. Soc.* **148** (2001) F35.
36. Zhang, H., Solanki, R., Roberds, B., Bai, G., and Banerjee, I., *J. Appl. Phys.* **87** (2000) 1921.
37. Kukli, K., Ritala, M., and Leskelä, M., *J. Appl. Phys.* **86** (1999) 5656.
38. Leskelä, M. and Ritala, M., *J. Phys. IV* **9** (1999) Pr8-837.
39. Haukka, S., Lakomaa, E.-L., and Suntola, T., *Stud. Surf. Sci. Catal.* **120** (1999) 715.
40. Fredriksson, F. and Carlsson, J.-O., *J. Chem. Vapor. Dep.* **1** (1993) 333.
41. Wilk, G.D., Wallace, R.M., and Anthony, J.M., *J. Appl. Phys.* **89** (2001) 5243.
42. Prengel, H.G., Pfouts, W.R., and Santhanam, A.T., *Surf. Coat. Technol.* **102** (1998) 183.
43. Gordon, R., *J. Non-Cryst. Solids* **218** (1997) 81.
44. Riihelä, D., Ritala, M., Matero, R., and Leskelä, M., *Thin Solid Films* **289** (1996) 250.
45. Edlou, S.M., Smajkiewicz, A., and Al-Jumaily, G.A., *Appl. Opt.* **32** (1993) 5601.
46. Suntola, T., *Thin Solid Films* **216** (1992) 84.
47. Shih, K.K. and Dove, D.B., *J. Vac. Sci. Technol. A* **12** (1994) 321.
48. Zborowski, J.T., Golding, T.D., Forrest, R.L., Marton, D., and Zhang, Z., *J. Vac. Sci. Technol. B* **16** (1998) 1451.

49. Hayama, K., Ishida, M., and Nakamura, T., *Jpn. J. Appl. Phys.* **33** (1994) 496.
50. Sawada, K., Ishida, M., Nakamura, T., and Ohtake, N., *Appl. Phys. Lett.* **52** (1988) 1672.
51. Ovsyannikov, V.P., Lashkarov, G.V., and Mazurenko, E.A., *J. Phys. IV* **5** (1995) 705.
52. Ciliberto, E., Fragalà, R., Rizza, R., Spoto, G., and Allen, G.C., *Appl. Phys. Lett.* **67** (1995) 1624.
53. Kim, J.S., Marzouk, H.A., Reucroff, P.J., Robertson, J.D., and Hamrin, Jr., C.E., *Appl. Phys. Lett.* **62** (1993) 681.
54. Zhao, Y.-W. and Suhr, H., *Appl. Phys. A* **55** (1992) 176.
55. Ritala, M., Kukli, K., Rahtu, A., Räsänen, P.I., Leskelä, M., Sajavaara, T., and Keinonen, J., *Science* **288** (2000) 319.
56. Ritala, M., Saloniemi, H., Leskelä, M., Prohaska, T., Friedbacher, G., and Grasserbauer, M., *Thin Solid Films* **286** (1996) 54.
57. Tiitta, M., *Doctoral (Tech.) thesis*, Helsinki University of Technology, Espoo 1998, 44p.
58. Matero, R., Rahtu, A., Ritala, M., Leskelä, M., and Sajavaara, T., *Thin Solid Films* **368** (2000) 1.
59. Kukli, K., Ritala, M., and Leskelä, M., *J. Vac. Sci. Technol. A* **15** (1997) 2214.
60. Yun, S.J., Lee, K-H., Skarp, J., Kim, H-R., and Nam, K-S., *J. Vac. Sci. Technol. A* **15** (1997) 2993.
61. Fleisher, M. and Meixner, H., *Sens. Actuators B* **5** (1991) 115.
62. Schwebel, T., Fleisher, M., and Meixner, H., *Sens. Actuators B* **65** (2000) 176.
63. Fleischer, M. and Meixner, H., *Sens. Actuators B* **6** (1992) 257.
64. Réti, F., Fleischer, M., Meixner, H., and Giber, J., *Sens. Actuators B* **18-19** (1994) 119.
65. Weh, T., Fleischer, M., and Meixner, H., *Sens. Actuators B* **68** (2000) 146.
66. Hoefler, U., Frank, J., and Fleischer, M., *Sens. Actuators B* **78** (2001) 6.
67. Minami, T., Shirai, T., Nakatani, T., and Miyata, T., *Thin Solid Films* **373** (2000) 145.
68. Minami, T., Nakatani, T., and Miyata, T., *J. Vac. Sci. Technol. A* **18** (2000) 1234.
69. Xiao, T., Kitai, A.H., Liu, G., Nakua, A., and Barbier, J., *Appl. Phys. Lett.* **72** (1998) 3356.
70. Hong, M., Lu, Z.H., Kwo, J., Kortan, A.R., Mannaerts, J.P., Krajewski, J.J., Hsieh, K.C., Chou, L.J., and Cheng, K.Y., *Appl. Phys. Lett.* **76** (2000) 312.

71. Kwo, J., Murphy, D.W., Hong, M., Opila, R.L., Mannaerts, J.P., Sergent, A.M., and Masaitis, R.L., *Appl. Phys. Lett.* **75** (1999) 1116.
72. Passlack, M., Hong, M., Mannaerts, J.P., Opila, R.L., Chu, S.N.G., Moriya, N., Ren, F., and Kwo, J.R., *IEEE Trans. Electron Devices* **44** (1997) 214.
73. Orita, M., Ohta, H., Hirano, M., and Hosono, H., *Appl. Phys. Lett.* **77** (2000) 4166.
74. Ogita, M., Saika, N., Nakanishi, Y., and Hatanaka, Y., *Appl. Surf. Sci.* **142** (1999) 188.
75. Macrí, P.P., Enzo, S., Sberveglieri, G., Groppelli, S., and Perego, C., *Appl. Surf. Sci.* **65/66** (1993) 277.
76. Fleischer, M. and Meixner, H., *Sens. Actuators B* **4** (1991) 437.
77. Fleischer, M., Hanrieder, W., and Meixner, H., *Thin Solid Films* **190** (1990) 93.
78. Hanrieder, W., Fleischer, M., and Meixner H., *J. Phys. D: Appl. Phys.* **22** (1989) 1938.
79. Passlack, M., Hunt, N.E.J., Schubert, E.F., Zydzik, G.J., Hong, M., Mannaerts, J.P., Opila, R.L., and Fischer, R.L., *Appl. Phys. Lett.* **64** (1994) 2715.
80. Passlack, M., Schubert, E.F., Hobson, W.S., Hong, M., Moriya, N., Chu, S.N.G., Konstadinidis, K., Mannaerts, J.P., Schnoes, M.L., and Zydzik, G.J., *J. Appl. Phys.* **77** (1995) 686.
81. Hariu, T., Sasaki, S., Adachi, H., and Shibata, Y., *Jpn. J. Appl. Phys.* **16** (1977) 841.
82. Battiston, G.A., Gerbasi, R., Porchia, M., Bertoncetto, R., and Caccavale, F., *Thin Solid Films* **279** (1996) 115.
83. Valet, M. and Hoffman, D.M., *Chem. Mater.* **13** (2001) 2135.
84. Míinea, L., Suh, S., Bott, S.G., Liu, J-R., Chu, W-K., and Hoffman, D.M., *J. Mater. Chem.* **9** (1999) 929.
85. Colombo, D.G., Gilmer, D.C., Young, V.G., Campell, S.A., and Gladfelter, W.L., *Chem. Vap. Deposition* **4** (1998) 220.
86. Ortiz, A., Alonso, J.C., Andrade, E., and Urbiola, C., *J. Electrochem. Soc.* **148** (2001) F26.
87. Kim, H-G. and Kim, W-T., *J. Appl. Phys.* **62** (1987) 2000.
88. Hoeneisen, B., Mead, C.A., and Nicolet, M-A., *Solid-State Electron.* **14** (1971) 1059.
89. Mahalingam, T., Radhakrishnan, M., and Balasubramanian, C., *Thin Solid Films* **78** (1981) 229.
90. De Asha, A.M. and Nix, R.M., *Surf. Sci.* **322** (1995) 41.
91. Kushkov, V.D., Zaslavskii, A.M., Zverlin, A.V., and Melnikov, A.V., *J. Mater. Sci. Lett.* **10** (1991) 1111.

92. Hass, G., Ramsey, J.B., and Thun, R., *J. Opt. Soc. Am.* **49** (1959) 116.
93. Singh, A., *Thin Solid Films* **105** (1983) 163.
94. Guha, S., Cartier, E., Gribelyuk, M.A., Bojarczuk, N.A., and Copel, M.C., *Appl. Phys. Lett.* **77** (2000) 2710.
95. Shiokawa, Y., Amano, R., Nomura, A., and Yagi, M., *J. Radioanal. Nucl. Chem.* **152** (1991) 373.
96. Weber, A. and Suhr, H., *Modern Phys. Lett. B* **3** (1989) 1001.
97. Suzuki, M., Kagawa, M., Syono, Y., and Hirai, T., *J. Cryst. Growth* **112** (1991) 621.
98. Gao, Y-M., Wu, P., Dwight, K., and Wold, A., *J. Solid State Chem.* **90** (1991) 228.
99. Wang, S., Wang, W., and Qian, Y., *Thin Solid Films* **372** (2000) 50.
100. Adachi, G-y and Imanaka, N., *Chem. Rev.* **98** (1998) 1479.
101. Eyring, L., in *Handbook on The Physics and Chemistry of Rare Earths*, Vol **3**, Gschneider Jr., K.A. and Eyring, L. (Eds.), North-Holland, Amsterdam 1979, 337.
102. Wu, Y.H., Yang, M-Y., Chin, A., Chen, W.J., and Kwei, C.M., *IEEE EDL* **21** (2000) 341.
103. Chin, A., Wu, Y.H., Chen, S.B., Liao, C.C., and Chen, W.J., *Tech. Dig. VLSI Symp.* (2000) 16.
104. Copel, M., Cartier, E., and Ross, F.M., *Appl. Phys. Lett.* **78** (2001) 1607.
105. Ono, H. and Katsumata, T., *Appl. Phys. Lett.* **78** (2001) 1832.
106. Aiyer, H.N., Raju, A.R., Subbanna, G.N., and Rao, C.N.R., *Chem. Mater.* **9** (1997) 755.
107. Carlson, C.M., Parilla, P.A., Siegal, M.P., Ginley, D.S., Wang, Y.-T., Blaugher, R.D., Price, J.C., Overmyer, D.L., and Venturini, E.L., *Appl. Phys. Lett.* **75** (1999) 2479.
108. Sagoi, M., Kinno, T., Yoshida, J., and Mizushima, K., *Appl. Phys. Lett.* **62** (1993) 1833.
109. Hedge, M.S., Satyalakshmi, K.M., Mallya, R.M., Rajeswari, M., and Zhang, H., *J. Mater. Res.* **9** (1994) 898.
110. Li, A., Ge, C., Lü, P., and Ming, N., *Appl. Phys. Lett.* **69** (1996) 161.
111. Meng, X.J., Cheng, J.G., Sun, J.L., Ye, H.J., Guo, S.L., and Chu, J.H., *J. Cryst. Growth* **220** (2000) 100.
112. Hwang, K.S. and Kim, B.H., *Appl. Surf. Sci.* **140** (1999) 231.
113. Kim, S.S., Kim, B.I., Park, Y.B., Kang, T.S., and Je, J.H., *Appl. Surf. Sci.* **169** (2001) 553.

114. Li, A., Ge, C., Lü, D., Xiong, S., and Ming, N., *Appl. Phys. Lett.* **70** (1997) 1616.
115. Srivastava, A., Kumar, D., and Singh, R.K., *Electrochem. Solid-State Lett.* **2** (1999) 294.
116. Chen, M-S., Wu, T-B., and Wu, J-M., *Appl. Phys. Lett.* **68** (1996) 1430.
117. Chao, G-C. and Wu, J-M., *Jpn. J. Appl. Phys.* **40** (2001) 1306.
118. Chen, P., Xu, S.Y., Zhou, W.Z., Ong, C.K., and Cui, D.F., *J. Appl. Phys.* **85** (1999) 3000.
119. Sánchez, F., Ferrater, C., Guerrero, C., Carcía-Cuenca, M.V., and Varela, M., *Appl. Phys. A* **71** (2000) 59.
120. Guo, X., Li, C., Zhou, Y., and Chen, Z., *J. Vac .Sci. Technol. A* **17** (1999) 917.
121. Yu, T., Chen, Y-F., Liu, Z-G., Chen, X-Y., Sun, L., Ming, N-B., and Shi, L-J., *Mater. Lett.* **26** (1996) 73.
122. Satyalakshmi, K.M., Mallya, R.M., Ramanathan, K.V., Wu, X.D., Brainard, B., Gautier, D.C., Vasanthacharya, N.Y., and Hedge, M.S., *Appl. Phys. Lett.* **62** (1993) 1233.
123. Yin, J., Chen, X.Y., Li, Q.C., Liu, X.Y., and Liu, Z.G., *J. Mater. Sci.* **33** (1998) 5631.
124. Sánchez, F., Ferrater, C., Alcobé, X., Bassas, J., Carcía-Cuenca, M.V., and Varela, M., *Thin Solid Films* **384** (2001) 200.
125. He, Q., Christen, D.K., Feenstra, R., Norton, D.P., Paranthaman, M., Specht, E.D., Lee, D.F., Goyal, A., and Kroeger, D.M., *Physica C* **314** (1999) 105.
126. Lee, H-Y., Wu, T-B., and Lee, J-F., *Jpn. J. Appl. Phys.* **36** (1997) 301.
127. Yang, C-C., Chen, M-S., Hong, T-J., Wu, C-M., Wu, J-M., and Wu, T-B., *Appl. Phys. Lett.* **66** (1995) 2643.
128. Hwang, K-S., Min, S-S., and Park, Y-J., *Surf. Coat. Technol.* **137** (2001) 205.
129. Ichinose, H., Shiwa, Y., and Nagano, M., *Jpn. J. Appl. Phys.* **33** (1994) 5907.
130. Cho, C.R., Payne, D.A., and Cho, S.L., *Appl. Phys. Lett.* **71** (1997) 3013.
131. Bao, D., Mizutani, N., Yao, X., and Zhang, L., *Appl. Phys. Lett.* **77** (2000) 1041.
132. Zou, Q., Ruda, H.E., and Yacobi, B.G., *Appl. Phys. Lett.* **78** (2001) 1282.
133. Meng, X-J., Sun, J-L., Yu, J., Ye, H-J., Guo, S-L., and Chu, J-H., *Appl. Surf. Sci.* **171** (2001) 68.
134. Li, A., Ge, C., Lü, P., and Ming, N., *Appl. Phys. Lett.* **68** (1996) 1347.
135. Gorbenko, O.Y., Kaul, A.R., Molodyk, A.A., Fuflyigin, V.N., Novozhilov, M.A., Bosak, A.A., Krause, U., and Wahl, G., *J. Alloys and Comp.* **251** (1997) 337.

136. Rebane, J.A., Gorbenko, Y.O., Suslov, S.G., Yakovlev, N.V., Korsakov, I.E., Amelichev, V.A., and Tretyakov, Y.D., *Thin Solid Films* **302** (1997) 140.
137. Hattori, T., Matsui, T., Tsuda, H., Mabuchi, H., and Morii, K., *Thin Solid Films* **388** (2001) 183.
138. Brosha, E.R., Mukundan, R., Brown, D.R., Garzon, F.H., Visser, J.H., Zanini, M., Zhou, Z., and Logothetis, E.M., *Sens. Actuators B* **69** (2000) 171.
139. Hwang, H.J., Moon, J., Awano, M., and Maeda, K., *J. Am. Ceram. Soc.* **83** (2000) 2852.
140. Jain, A.N., Tiwari, S.K., Singh, R.N., and Chartier, P., *J.Chem.Soc. Faraday Trans.* **91** (1995) 1871.
141. Zhang, Y., Zhu, Y., Tan, R., Yao, W., and Cao, L., *Thin Solid Films* **388** (2001) 160.
142. Ichinose, H., Katsuki, H., and Nagano, M., *J. Cryst. Growth* **144** (1994) 59.
143. Matsumoto, Y., Sasaki, T., and Hombo, J., *Inorg. Chem.* **31** (1992) 738.
144. Lee, J., Choi, C.H., Park, B.H., Noh, T.W., and Lee, J.K., *Appl. Phys. Lett.* **72** (1998) 3380.
145. Gunasekaran, R.A., Pedarnig, J.D., and Dinescu, M., *Appl. Phys. A* **69** (1999) 621.
146. Shimixu, Y., Ishikawa, A., Iseki, K., and Takase, S., *J. Electrochem. Soc.* **147** (2000) 3931.
147. Geller, S. and Bala, V.B., *Acta Cryst.* **9** (1956) 1019.
148. Konaka, T., Sato, M., Asano, H., and Kubo, S., *J. Supercond.* **4** (1991) 283.
149. Zuccaro, C., Winter, M., Klein, N., and Urban, K., *J. Appl. Phys.* **82** (1997) 5695.
150. Malandrino, G., Frassica, A., Condorelli, G.G., Lanza, G., and Fragalá, I.L., *J. Alloys Compd.* **251** (1997) 314.
151. Meng, X.F., Pierce, F.S., Wong, K.M., Amos, R.S., Xu, C.H., Deaver Jr., B.S., and Poon, S.J., *IEEE Trans. Magn.* **27** (1991) 1638.
152. Schneidewind, H., Manzel, M., Bruchlos, G., and Kirsc, K., *Supercond. Sci. Technol.* **14** (2001) 200.
153. Phillips, J.M., *J. Appl. Phys.* **79** (1996) 1829.
154. Carlson, C.M., Price, J.C., Parilla, P.A., Ginley, D.S., Niles, D., Blaugher, R.D., Goyal, A., Paranthaman, M., Kroeger, D.M., and Christen, D.K., *Physica C* **304** (1998) 82.
155. Shoup, S.S., Paranthaman, M., Goyal, A., Specht, E.D., Lee, D.F., Kroeger, D.M., and Beach, D.B., *J. Am. Ceram. Soc.* **81** (1998) 3019.

156. Molodyk, A.A., Korsakov, I.E., Novojilov, M.A., Graboy, I.E., Kaul, A.R., and Wahl, G., *Chem. Vap. Deposition* **6** (2000) 133.
157. Malandrino, G. and Fragalá, I.L., *Chem. Mater.* **10** (1998) 3765.
158. Malandrino, G. and Fragalá, I.L., *Electrochem. Soc. Proc.* **97-25** (1997) 844.
159. Malandrino, G., Frassica, A., and Fragalá, I.L., *Chem. Vap. Deposition* **3** (1997) 306.
160. Cabañas, M.V., Ragel, C.V., Conde, F., González-Calbet, J.M., and Vallet-Regí, M., *Solid State Ionics* **101-103** (1997) 191.
161. Sandu, V., Jaklovszky, J., Miu, D., Drăgălinescu, D., Grigoriu, C., and Bunescu, M.C., *J. Mater. Sci. Lett.* **13** (1994) 1222.
162. Sader, E., *Supercond. Sci. Technol.* **6** (1993) 647.
163. Sader, E., Schmidt, H., Hradil, K., and Wersing, W., *Supercond. Sci. Technol.* **4** (1991) 371.
164. Lee, A.E., Platt, C.E., Bursch, J.F., Simon, R.W., Goral, J.P., and Al-Jassim, M.M., *Appl. Phys. Lett.* **57** (1990) 2019.
165. Shoup, S.S., Paranthaman, M., Beach, D.B., Specht, E.D., and Williams, R.K., *J. Mater. Res.* **12** (1997) 1017.
166. Ng, M.F. and Cima, M.J., *J. Mater. Res.* **12** (1997) 1306.
167. Peshev, P. and Slavova, V., *Mater. Res. Bull.* **29** (1994) 255.
168. Giess, E.A., Sandstrom, R.L., Gallager, W.J., Gupta, A., Shinde, S.L., Cook, R.F., Cooper, E.I., O'Sullivan, E.J.M., Roldan, J.M., Segmüller, A.P., and Angilello, J., *IBM J. Res. Develop.* **34** (1990) 916.
169. Vasylechko, L., Matkovski, A., Suchocki, A., Savytskii, D., and Syvorotka, I., *J. Alloys Compd.* **286** (1999) 213.
170. Howard C.J. and Kennedy, B.J., *J. Phys. Condens. Matter.* **11** (1999) 3229.
171. Miyazawa, S., *Appl. Phys. Lett.* **55** (1989) 2230.
172. Ishihara, T., Matsuda, H., and Takita, Y., *J. Am. Chem. Soc.* **116** (1994) 3801.
173. Morrell, J.S., Xue, Z.B., Specht E.D., and Beach, D.B., *Mat. Res. Soc. Symp. Proc.* **547** (1999) 309.
174. Kagawa, K., Arimura, M., Nagano, M., and Syono, Y., *Adv. Sci. Technol. (Faega, Italy, Surface Eng.)* **20** (1999) 241.
175. Belcher, R., Jenkins, C.R., Stephen, I., and Uden, P.C., *Talanta* **17** (1970) 455.
176. Eisentraut, K.J. and Sievers, R.E., *J. Am. Chem. Soc.* **87** (1965) 5256.
177. Suntola, T., Pakkanen, A., and Lindfors, S., *US Patent No.* 4,389,973 (1983).



178. Ylilammi, M. and Ranta-aho, T., *Thin Solid Films* **232** (1993) 56.
179. Putkonen, M., Johansson, L.-S., Sajavaara, T., and Niinistö, L. *Chem. Vap. Deposition* **7** (2001) 44.
180. Kukli, K., Heikkinen, H., Nykänen, E., and Niinistö, L., *J. Alloys. Comp.* **275-277** (1998) 10.
181. Utriainen, M., Kröger-Laukkanen, M., and Niinistö, L., *Mater. Sci. Eng. B* **54** (1998) 98.
182. Haukka, S., Lindblad, M., and Suntola, T., *Appl. Surf. Sci.* **112** (1997) 23.
183. Rousseau, F., Jain, A., Kodas, T., Hampden-Smith, M., Doug Farr, J., and Muenchausen, R., *J. Mater. Chem.* **2** (1992) 893.
184. Nieminen, M., *Licentiate (Tech.) thesis*, Helsinki University of Technology, Department of Chemical Engineering, Espoo 1995, 76 p.
185. Iida, K. and Tsujide, T., *Jpn.J.Appl.Phys.* **11** (1972) 840.
186. Hiltunen, L., Kattelus, H., Leskelä, M., Mäkelä, M., Niinistö, L., Nykänen, E., Soininen, P. and Tiitta, M., *Mater. Chem. Phys.* **28** (1991) 379.
187. Bernal, S., Diaz, J.A., Garcia, R., and Rodriguez-Izquierdo, J.M., *J. Mater. Sci.* **20** (1985) 537.
188. Nilsen, O., Peussa, M., Fjellvåg, H., Niinistö, L., and Kjekshus, A., *J. Mater. Chem.* **9** (1999) 1781.
189. Putkonen, M., Johansson, L.-S., Rauhala, E., and Niinistö, L., *J. Mater. Chem.* **9** (1999) 2449.
190. Putkonen, M., Sajavaara, T., and Niinistö, L., *J. Mater. Chem.* **10** (2000) 1857.